

# Journal Pre-proof

$\gamma\delta$  intraepithelial lymphocytes facilitate pathological epithelial cell shedding via CD103-mediated granzyme release.

Madeleine D. Hu, Natasha B. Golovchenko, Grace L. Burns, Prema M. Nair, Thomas J. Kelly, IV, Jonathan Agos, Mudar Zand Irani, Wai Sinn Soh, Matthew R. Zeglinski, Alexander Lemenze, Edward M. Bonder, Inga Sandroock, Immo Prinz, David J. Granville, Simon Keely, Alastair J.M. Watson, Karen L. Edelblum

PII: S0016-5085(21)03804-X  
DOI: <https://doi.org/10.1053/j.gastro.2021.11.028>  
Reference: YGAST 64723

To appear in: *Gastroenterology*  
Accepted Date: 19 November 2021

Please cite this article as: Hu MD, Golovchenko NB, Burns GL, Nair PM, Kelly IV TJ, Agos J, Irani MZ, Soh WS, Zeglinski MR, Lemenze A, Bonder EM, Sandroock I, Prinz I, Granville DJ, Keely S, Watson AJM, Edelblum KL,  $\gamma\delta$  intraepithelial lymphocytes facilitate pathological epithelial cell shedding via CD103-mediated granzyme release., *Gastroenterology* (2021), doi: <https://doi.org/10.1053/j.gastro.2021.11.028>.

This is a PDF file of an article that has undergone enhancements after acceptance, such as the addition of a cover page and metadata, and formatting for readability, but it is not yet the definitive version of record. This version will undergo additional copyediting, typesetting and review before it is published in its final form, but we are providing this version to give early visibility of the article. Please note that, during the production process, errors may be discovered which could affect the content, and all legal disclaimers that apply to the journal pertain.

© 2021 by the AGA Institute



**Hu et al.**

**$\gamma\delta$  intraepithelial lymphocytes facilitate pathological epithelial cell shedding via CD103-mediated granzyme release.**

**Lay summary:** Sentinel tissue-resident T cells facilitate the extrusion of epithelial cells undergoing programmed cell death in response to pro-inflammatory signals via integrin-mediated extracellular serine protease release.

**What you need to know:**

**BACKGROUND AND CONTEXT:** Excessive shedding of apoptotic enterocytes into the intestinal lumen is correlated with relapse in inflammatory bowel disease, yet the role of intraepithelial lymphocytes in this process is not well understood.

**NEW FINDINGS:**  $\gamma\delta$  intraepithelial lymphocytes make extended contact with shedding apoptotic enterocytes and facilitate this process through CD103 ( $\alpha_E\beta_7$  integrin)-mediated release of extracellular granzymes.

**LIMITATIONS:**  $\gamma\delta$  intraepithelial lymphocytes are not required for TNF-induced apoptosis.

**IMPACT:** Targeting CD103 or using a pan- $\beta_7$  inhibitor may be a viable approach to control excessive TNF-induced cell shedding and prevent relapse in Crohn's disease patients.

**$\gamma\delta$  intraepithelial lymphocytes facilitate pathological epithelial cell shedding via CD103-mediated granzyme release.**

Madeleine D. Hu<sup>1</sup>, Natasha B. Golovchenko<sup>1</sup>, Grace L. Burns<sup>2</sup>, Prema M. Nair<sup>2</sup>, Thomas J. Kelly IV<sup>1</sup>, Jonathan Agos<sup>1</sup>, Mudar Zand Irani<sup>2</sup>, Wai Sinn Soh<sup>2</sup>, Matthew R. Zeglinski<sup>3</sup>, Alexander Lemenze<sup>1</sup>, Edward M. Bonder<sup>4</sup>, Inga Sandrock<sup>5</sup>, Immo Prinz<sup>6</sup>, David J. Granville<sup>3</sup>, Simon Keely<sup>2</sup>, Alastair J.M. Watson<sup>7</sup>, Karen L. Edelblum<sup>1</sup>

<sup>1</sup>Center for Immunity and Inflammation, Department of Pathology, Immunology & Laboratory Medicine, Rutgers New Jersey Medical School, Newark, NJ, 07103, USA

<sup>2</sup>NHMRC Centre of Research Excellence in Digestive Health, College of Health, Medicine and Wellbeing, University of Newcastle, Callaghan, NSW, 2308, Australia, Hunter Medical Research Institute, Lot 1 Kookaburra Circuit, New Lambton Heights, NSW, 2305, Australia

<sup>3</sup>Department of Pathology and Laboratory Medicine, University of British Columbia, Vancouver, British Columbia, V6T 2B5, Canada

<sup>4</sup>Department of Biological Sciences, Rutgers University – The State University of New Jersey, Newark, NJ, 07102, USA

<sup>5</sup>Institute of Immunology, Hannover Medical School, Hannover, Germany

<sup>6</sup>Institute of Systems Immunology, University Medical Center Hamburg-Eppendorf, 20246 Hamburg, Germany

<sup>7</sup>Department of Gastroenterology and Gut Biology, Norwich Medical School, University of East Anglia, Norwich, UK

**Short title:**  $\gamma\delta$  IELs facilitate enterocyte shedding

**Acknowledgments:** The authors would like to thank Jerry Turner for providing the mRFP-ZO-1 Tg mice, Juan Flores for assistance with embedding, Raj Patel for thin sectioning for electron microscopy, Laureate Professor Nicholas J. Talley for advice and resources, and Kyra Minahan for histological support. We also gratefully acknowledge Angela Patterson for her thoughtful input. Electron microscopy was performed in the AICF at Rutgers-Newark. Cell sorting was performed at the NJMS Flow Cytometry and Immunology Core Laboratory and supported by National Institute for Research Resources Grant S10RR027022. This work was supported by National Institute of Health Grants R21AI143892 (K.L.E.), T32AI125185, F30DK121391 (M.D.H.) and the New Jersey Health Foundation (K.L.E.), grants BB/J004529/1 and BB/K018256/1 (A.J.M.W.), and NHMRC Project grant and CRE Digestive Health (S.K.). D.J.G. was funded by a Canadian Institutes for Health Research Foundation Grant.

**Abbreviations:** basement membrane, BM; cleaved caspase-3, CC3; diphtheria toxin, DT; granzyme, Gzm; inflammatory bowel disease, IBD; interleukin, IL; intraepithelial lymphocyte, IEL; knockout, KO; lateral intercellular space, LIS; lipopolysaccharide, LPS; tumor necrosis factor, TNF; T cell receptor, TCR; zona occludens-1, ZO-1

**Correspondence:** Karen Edelblum, Ph.D., 205 South Orange Ave, Cancer Center G1228, Newark, NJ 07103, tel: 973-972-3071; ke163@njms.rutgers.edu

**Disclosures:** The authors declare no competing financial interests.

**Author contributions:** M.D.H. performed experiments and wrote the manuscript. N.B.G. performed experiments and reviewed the manuscript. T.J.K., J.A., E.M.B., P.M.N., G.L.B., M.Z.I, W.S.S., A.L. performed experiments. M.R.Z., I.S., I.P., D.J.G., S.K. provided resources for the study and reviewed the manuscript. A.J.M.W. conceived the study, contributed to experimental design and reviewed the manuscript. K.L.E. conceived the study, performed experiments, supervised the research and wrote the manuscript.

**Data transparency statement:** Mice and published data will be made available freely without requirements or conditions on use other than those specified in standard Material Transfer Agreements.

**Preprint:** <https://doi.org/10.1101/2021.01.20.427150>

## **Abstract**

**Background & Aims:** Excessive shedding of apoptotic enterocytes into the intestinal lumen is observed in inflammatory bowel disease and is correlated with disease relapse. Based on their cytolytic capacity and surveillance behavior, we investigated whether intraepithelial lymphocytes expressing the  $\gamma\delta$  T cell receptor ( $\gamma\delta$  IELs) are actively involved in the shedding of enterocytes into the lumen.

**Methods:** Intravital microscopy was performed on GFP  $\gamma\delta$  T cell reporter mice treated with intraperitoneal (i.p.) lipopolysaccharide (LPS, 10 mg/kg) for 90 min to induce tumor necrosis factor (TNF)-mediated apoptosis. Cell shedding in various knockout or transgenic mice in the presence or absence of blocking antibody was quantified by immunostaining for ZO-1 junctions and cleaved caspase-3 (CC3). GzmA and GzmB release from *ex vivo* stimulated  $\gamma\delta$  IELs was quantified by ELISA. Immunostaining for  $\gamma\delta$  T cell receptor (TCR) and CC3 was performed on duodenal and ileal biopsies from control and Crohn's disease patients.

**Results:** Intravital microscopy of LPS-treated mice revealed that  $\gamma\delta$  IELs make extended contact with shedding enterocytes. These prolonged interactions require CD103 engagement by E-cadherin, and CD103 knockout or blockade significantly reduced LPS-induced shedding. Furthermore, we find that granzymes A and B, but not perforin, are required for cell shedding. These extracellular granzymes are released by  $\gamma\delta$  IELs both constitutively and following CD103/E-cadherin ligation. Moreover, we find that the frequency of  $\gamma\delta$  IEL localization to CC3-positive enterocytes is increased in Crohn's disease biopsies compared to healthy controls.

**Conclusion:** Our results uncover a previously unrecognized role for  $\gamma\delta$  IELs in facilitating TNF-mediated shedding of apoptotic enterocytes via CD103-mediated extracellular granzyme release.

Keywords: mucosal immunology, gamma delta T cells, cell extrusion

## **Introduction**

The intestinal epithelium is a single cell layer that serves as a critical barrier to prevent interaction between luminal contents and the mucosal immune system<sup>1</sup>. The maintenance of the small intestinal epithelial barrier is dependent upon tight regulation between proliferation in the crypt and shedding, or extrusion of epithelial cells, at the villus tip<sup>2</sup>. While physiological cell shedding at steady-state is required to maintain epithelial homeostasis, the rate of shedding is significantly enhanced in inflammatory bowel disease (IBD)<sup>3, 4</sup>. In this context, pathological shedding results in the loss of multiple contiguous epithelial cells, which can lead to ulceration or allow entry of luminal antigen and bacteria into the underlying tissue, thus inducing inflammation.

IBD is a multi-factorial disease that affects 6.8 million individuals worldwide<sup>5</sup>. Overproduction of tumor necrosis factor (TNF) is a hallmark of intestinal inflammation in IBD<sup>6</sup>, and therefore, anti-TNF antibodies are widely used therapeutically<sup>7</sup>. While approximately one-third of these patients achieve clinical remission with anti-TNF therapy, one-third of patients exhibit only an intermediate response, and the remaining one-third are non-responsive. Since a substantial increase in cell shedding is a known predictor of relapse in Crohn's disease (CD) patients<sup>8</sup>, it may be possible to enhance or supplement the clinical response to anti-TNF therapy in intermediate responders by identifying additional mechanisms that regulate shedding events.

Pathological cell shedding can be modeled in mice through the systemic administration of pro-inflammatory mediators such as TNF or lipopolysaccharide (LPS)<sup>9, 10</sup>. Both stimuli induce apoptosis and thus excessive cell shedding in mice through an epithelial TNFR1-dependent signaling mechanism. These TNF-mediated shedding events can be identified by caspase-3 activation and the formation of an actomyosin funnel that surrounds the shedding cell as it is extruded<sup>10</sup>. Nuclear fragmentation is observed once the cell is extruded into the lumen. While cytoskeletal remodeling and caspase activation are critical for the shedding process<sup>10</sup>, much remains unknown regarding the mechanisms by which individual cells are targeted for extrusion or the contribution of direct interactions with immune cells to this process.

Intraepithelial lymphocytes (IELs) expressing the  $\gamma\delta$  T cell receptor (TCR) bridge innate and adaptive immunity, exhibit a largely protective response to dampen acute inflammation and promote mucosal barrier integrity<sup>11</sup>. Further,  $\gamma\delta$  IELs also contribute to epithelial turnover and proliferation in response to injury<sup>12, 13</sup>. We have previously shown that  $\gamma\delta$  IELs provide immune surveillance of the villous epithelium by migrating along the basement membrane (BM) and between adjacent epithelial cells in the lateral intercellular space (LIS)<sup>14, 15</sup>. This motility is dependent upon ligand-binding interactions between the IEL and enterocyte, with CD103 ( $\alpha_E\beta_7$  integrin)/E-cadherin binding being critical for the

retention of  $\gamma\delta$  IELs within the LIS.

Although epithelial apoptosis can be induced through cytolytic functions of IELs, the role of  $\gamma\delta$  IELs in pathological cell shedding has yet to be investigated. Herein, we have used intravital microscopy to demonstrate that  $\gamma\delta$  IELs make prolonged contacts with enterocytes prior to their extrusion in LPS-treated mice. These extended cell-cell contacts are dependent upon CD103 ligation, and both genetic ablation and antibody-mediated blockade of CD103 reduce the severity of LPS-induced cell shedding. Further, we show that  $\gamma\delta$  IEL-derived granzymes A and B, which are secreted both at steady-state and in response to CD103 engagement, are required for apoptotic cell shedding. This process is perforin-independent, indicating that CD103 ligation stimulates the extracellular release of granzymes by  $\gamma\delta$  IELs. Additionally, we observe that the association between  $\gamma\delta$  IELs and CC3<sup>+</sup> enterocytes is increased in biopsies from Crohn's disease patients. These findings represent a previously undiscovered role for  $\gamma\delta$  IELs in facilitating cell shedding and may provide a novel therapeutic target to maintain mucosal homeostasis during remission in IBD patients.

## **Materials and methods**

Additional methods including immunostaining, electron microscopy, flow cytometry, qPCR and ELISA can be found in Supplementary Materials.

### **Animals**

Mice of both sexes were used at 8-13 weeks of age and maintained on a C57BL/6 background under specific pathogen-free (SPF) conditions in Allentown caging with aspen shavings and LabDiet 5010 chow (Purina, St. Louis, MO). Wildtype, Tcrd knockout (KO)<sup>16</sup>, and Prf1 KO mice were obtained from the Jackson Laboratory. TcrdH2BEGFP (TcrdEGFP) mice<sup>17</sup> were provided by Bernard Malissen (INSERM) and crossed to CD103 KO (Jackson Labs) or mRFP-ZO1 Tg mice generously provided by Jerrold Turner (Harvard BWH)<sup>18</sup>. TcrdGDL mice<sup>19</sup> were provided by Immo Prinz and Inga Sandrock (Hannover). GzmA/GzmB double knockout mice were provided by Todd Fehniger (WashU), and bones from GzmK and GzmB KO mice were obtained from David Granville (UBC). All studies were conducted in an Association of the Assessment and Accreditation of Laboratory Animal Care–accredited facility according to protocols approved by Rutgers New Jersey Medical School Comparative Medicine Resources. To induce  $\gamma\delta$  T cell depletion in TcrdGDL mice, 15 ng of diphtheria toxin (List Biological, Campbell, CA) per gram body weight was administered i.p. 24 and 48 h prior to the experiment.

### **Shedding assays**

Mice were injected intraperitoneally with 10 mg/kg of LPS from *E. coli* O111:B4 (Sigma-Aldrich, St. Louis, MO) or 7.5  $\mu\text{g}$  of recombinant TNF (Peprotech, East Windsor, NJ) and euthanized after 90 min. Where indicated, mice were pre-treated with 150  $\mu\text{g}$  anti-CD103 (M290, BioXcell, Lebanon, NH) or 200  $\mu\text{g}$  of anti-NKG2D (HMG2D, BioXcell) 1 h prior to LPS treatment; or 2 x 200  $\mu\text{g}$  anti-TCR $\gamma\delta$  (UC7-13D5, BioXcell) 24 and 48h prior to LPS treatment. Rat IgG2a (RTK2758, BioLegend) or Armenian hamster IgG (BioXcell) were used as controls. 100  $\mu\text{g}$  propidium iodide (Thermo Fisher Scientific, Beverly, MA) was administered i.v. prior to euthanasia. As a control for pyroptosis, 0.16  $\mu\text{g}/\text{g}$  PA and 0.08  $\mu\text{g}/\text{g}$  LFn-Fla (*L. pneumophila* flagellin, provided by Isabella Rauch (OHSU)) was administered i.v. for 60 min<sup>20</sup>. To quantify shedding events, immunohistochemistry was performed as described in supplementary materials. Positive shedding events were identified via ZO-1 funnels, CC3 staining and/or cellular morphology.

### **Intravital microscopy**

Intravital imaging was performed as previously described<sup>21,22</sup>. For some experiments, APC-CD8 $\alpha$  (10  $\mu$ g, 53-6.7, eBioscience) was injected i.v. at the same time as LPS treatment and AlexaFluor 568 (Life Technologies, Carlsbad, CA) was used as a luminal marker. Imaris (v. 9.6, Bitplane, South Windsor, CT) was used to render 3D reconstructions and apply an autoregressive tracking algorithm to enable quantification of IEL motility. IEL contact with shedding cells was manually quantified and verified using both 3D maximum intensity projections and single slices of a z-stack. Dwell time indicates the duration of a single IEL/epithelial contact.

### **Generation of bone marrow chimeras**

8-week-old Tcrd KO mice were exposed to 11 Gy of gamma irradiation. 24 hours later, irradiated mice were retro-orbitally injected with  $5 \times 10^6$  bone marrow cells from donor mice. Mixed bone marrow chimeras (80/20) were generated by engrafting  $4 \times 10^6$  Tcrd KO and  $1 \times 10^6$  WT, GzmA/B KO or CD103 KO bone marrow cells. Tissue was harvested 8 weeks post-engraftment.

### **Halo analysis of $\gamma\delta$ TCR and caspase dual IHC staining**

All studies were performed in accordance with the Hunter New England Local Health District Human Ethics Committee (AU202003-12 and 2020/ETH03303). Slides were digitized using the Aperio AT2 (Leica Biosystems, Mount Waverley, Australia), and  $\gamma\delta$ TCR and CC3 staining intensities in each section were scored histologically using the HALO software area quantification algorithm (Indica Labs, Albuquerque, NM). Total  $\gamma\delta$ TCR (DAB) and CC3 (alkaline phosphatase (AP)) staining was quantified in 5 representative villi per section. The pixel intensity score was used to calculate a HALO (H)-score: (3 x % of pixels with strong intensity) + (2 x % of pixels with moderate intensity) + (1 x % of pixels with weak intensity). The H-score for  $\gamma\delta$ TCR was normalized against the total number of  $\gamma\delta$  IELs to account for differences in cell number per analyzed villus. The H-score for CC3 was normalized by the total area analyzed ( $\mu\text{m}^2$ ) to account for variation in villus size. For each section, CC3-associated  $\gamma\delta$  T cells were represented as CC3 per area per  $\gamma\delta$  IEL.

### **Statistical analyses**

Statistical analysis was performed using GraphPad Prism (San Diego, CA). Two-tailed unpaired Student *t* tests were used to directly compare two independent samples;  $p \leq 0.05$  was considered statistically significant. Comparisons between

multiple independent variables were performed using one-way ANOVA followed by post-hoc Tukey multiple comparisons tests. The two-stage Benjamini, Krieger, and Yekutieli procedure was used post hoc to control the false discovery rate. All data are presented as either the mean  $\pm$  SEM or with a 95% confidence interval.

Journal Pre-proof

## **Results**

### **$\gamma\delta$ IELs directly interact with shedding cells in response to lipopolysaccharide.**

Previously published electron microscopy studies observed IELs located directly beneath or adjacent to shedding enterocytes under homeostatic conditions<sup>23</sup>. While it was hypothesized that IELs may plug the gap left behind by the extruded cell, recent studies provide conclusive evidence that neighboring epithelial cells extend protrusions underneath the shedding cell to maintain an intact epithelial monolayer<sup>10</sup>. Although these studies have elucidated many of the epithelial cell-intrinsic intracellular signals involved in coordination of the shedding process, whether IELs are actively involved in the shedding of enterocytes into the lumen remains unclear.

To determine whether IELs contact shedding cells in the context of inflammation, we treated wildtype (WT) mice with LPS for 90 min to rapidly induce apoptotic cell shedding, as quantified by cellular morphology and cleaved caspase-3 (CC3)-positive staining (Fig. 1A,B)<sup>9</sup>. We then used transmission electron microscopy to examine jejunal villi from LPS-treated mice (Fig. 1C) and identified multiple instances in which IELs were in direct contact with shedding events. Using mice expressing a Tcrd-histone 2B enhanced GFP reporter (TcrdEGFP)<sup>17</sup>, we found that GFP<sup>+</sup>  $\gamma\delta$  IELs were near CC3<sup>+</sup> shedding events following LPS exposure (Fig 1D).

We next performed intravital microscopy on the jejunal mucosa of LPS-treated TcrdEGFP mice to examine the spatiotemporal dynamics of IEL-shedding enterocyte interactions. This technique enabled us to observe shedding cells as they were extruded into the lumen as well as  $\gamma\delta$  IEL surveillance behavior<sup>14</sup>. We found that approximately 46% of shedding cells were contacted by a  $\gamma\delta$  IEL prior to their extrusion (Fig. 2A, Video S1), and that the  $\gamma\delta$  IELs contacting shedding events migrated at slower speeds relative to  $\gamma\delta$  IELs that did not (Fig. 2B). This reduced migratory speed is likely attributable to the increased dwell time of  $\gamma\delta$  IELs at the base of shedding enterocytes (Fig. 2C). Interestingly, we did not observe CD8<sup>+</sup> TCR $\alpha\beta$ <sup>+</sup>(GFP<sup>-</sup>) IELs associating with shedding events in LPS-treated mice (Video S2), indicating that these interactions may be unique to  $\gamma\delta$  IELs. We next asked whether  $\gamma\delta$  IELs also interact with shedding events under steady-state conditions by analyzing 8 videos acquired from untreated TcrdEGFP mice. As expected, the relative frequency of cell extrusion in the jejunum of untreated mice was rare; however, we found that in 7 of the 24 shedding events observed (29%), a  $\gamma\delta$  IEL contacted the enterocyte immediately prior to its extrusion.

The shedding of apoptotic enterocytes in response to inflammatory stimuli is a well-defined process that begins with junction protein rearrangement and formation of an actin funnel and concludes with extrusion of the cell into the

lumen<sup>10</sup>. To determine when in this process  $\gamma\delta$  IELs contact the shedding cell, intravital microscopy was performed on mice expressing both a Tcrd cytoplasmic eGFP reporter (TcrdGDL)<sup>19</sup> and a monomeric RFP (mRFP)-zonula occludens 1 (ZO-1) fusion protein<sup>18</sup>. We find that  $\gamma\delta$  IELs interact with shedding cells prior to the formation of the actin funnel (Fig. 2D, Video S3), indicating that IELs are present during or shortly after initiation of the shedding process.

### **CD103 is required for TNF-mediated shedding of apoptotic enterocytes.**

The extended contact between  $\gamma\delta$  IELs and shedding enterocytes led us to investigate whether IEL dwell time at sites of cell shedding was critical to the extrusion process. We have previously shown that loss of CD103 increases  $\gamma\delta$  IEL motility by reducing dwell time in the LIS, likely through disruption of CD103/E-cadherin interactions<sup>14, 15</sup>. Thus, to determine whether altering the duration of IEL/epithelial contact affects cell shedding, we investigated the extent of cell extrusion in LPS-treated WT and CD103-deficient mice. At the peak of shedding, CD103 knockout (KO) mice exhibited a reduced number of CC3<sup>+</sup> cells relative to WT mice throughout the small intestine (Fig. 1A, 3A,B, S1A). Loss of CD103 also abrogated LPS-induced shedding at later timepoints, indicating that the marked reduction in CC3<sup>+</sup> cells was not due to a delayed response (data not shown). Similarly, CD103 KO mice exhibited a substantial reduction in shedding relative to WT in response to high dose TNF (Fig. 3C), confirming that loss of CD103 confers protection against TNFR-dependent shedding events<sup>9, 10</sup>. Notably, villi in CD103 KO mice were longer than those in WT mice, supporting a role for  $\gamma\delta$  IELs in physiological shedding (Fig. S1B). Actomyosin contraction can occur in the absence of caspase activation<sup>10</sup>, however, we did not observe an increase in CC3<sup>-</sup> funnels (Fig. S1C). Moreover, the extruding enterocytes are not permeable to propidium iodide, suggesting that these cells do not undergo an alternative form of cell death, such as necroptosis or pyroptosis (Fig S1D). Together, these data support our observation that  $\gamma\delta$  IELs directly contact apoptotic enterocytes during the initial stage of shedding, an interaction dependent upon CD103 ligation with E-cadherin.

We assessed whether differences in the microbiome contributed to the reduced cell shedding observed in CD103 KO mice; however, cohousing had no appreciable effect on the protection conferred by loss of CD103 (Fig. S1E). Although CD103 promotes migration of  $\gamma\delta$  IELs and other TNF-producing immune cells into and within the gut, intestinal TNF levels were similar in LPS-treated WT and CD103 KO mice (data not shown). These findings indicate that the decrease in LPS-induced apoptosis observed in CD103-deficient mice cannot be attributed to reduced mucosal TNF production or an altered microbiome.

To evaluate  $\gamma\delta$  IEL interactions with the few shedding events that do occur in absence of CD103, we performed intravital microscopy on LPS-treated TcrdEGFP; CD103 KO mice. As expected,  $\gamma\delta$  IELs contact shedding cells in CD103 KO mice less frequently than in WT (Fig. 3D) and the few  $\gamma\delta$  IELs that interacted with shedding enterocytes migrated more rapidly and exhibited reduced dwell times at these shedding events as compared to their WT counterparts (Fig. 3E, S1F). Next, we investigated whether blocking CD103 interaction with its binding partner, E-cadherin, is sufficient to reduce apoptotic cell shedding. Mice treated with anti-CD103 (Fig. S1G) exhibited a 50% decrease in LPS-induced cell shedding compared to mice receiving an isotype control (Fig. 3F). Similar to our findings in CD103 KO mice, these reductions in LPS-induced cell shedding were not accompanied by reduced TNF production (data not shown). Together, these data demonstrate a requirement for CD103 binding in the extrusion process and show that short-term blockade of CD103 is sufficient to reduce the frequency of apoptotic shedding events.

To determine whether CD103 expressed specifically on  $\gamma\delta$  IELs was responsible for facilitating LPS-induced shedding, we attempted to generate mixed bone marrow chimeras by engrafting lethally-irradiated  $\gamma\delta$  T-cell-deficient (Tcrd KO) mice with 80% Tcrd KO and 20% CD103 KO or WT bone marrow. CD103 plays an important role in lymphocyte gut homing<sup>24</sup>. We do not observe a reduction in  $\gamma\delta$  IEL number in our CD103 KO colony, yet we found that CD103-deficient  $\gamma\delta$  T cells were unable to repopulate the IEL niche to a comparable level as WT (Fig. S1H). Although we were unable to directly assess the contribution of  $\gamma\delta$  IEL CD103 to cell shedding, our findings demonstrate a novel role for CD103 in mediating TNF-induced shedding of apoptotic cells and show that antibody-mediated blockade of  $\alpha_E$  integrin reduces the severity of the shedding response.

### **$\gamma\delta$ IELs are not required for LPS-induced cell shedding.**

Previous studies have demonstrated that adaptive immunity can limit the extent of TNF-induced epithelial apoptosis<sup>25</sup>; however, the specific contribution of  $\gamma\delta$  T cells to the shedding of apoptotic cells has not been addressed. To this end, we first quantified LPS-induced cell shedding in WT and Tcrd KO mice and observed no difference in either the frequency of CC3<sup>+</sup> cells (Fig. 4A). Surprisingly, we found that enterocytes are extruded more rapidly following LPS treatment of Tcrd KO mice, compared to WT (Fig. 4B). Further, there was a slight reduction in the extrusion rate of enterocytes that interact with  $\gamma\delta$  IELs compared to those that did not in WT mice. These data indicate that apoptotic enterocytes interacting with  $\gamma\delta$  IELs are extruded from the monolayer more slowly, suggesting a potential subdivision of apoptotic cell shedding events.

Since the loss of  $\gamma\delta$  T cells can be partially compensated other immune cells with similar functions<sup>19</sup>, we next evaluated LPS-induced cell shedding following inducible depletion of  $\gamma\delta$  T cells. Mice homozygous for the diphtheria toxin (DT) receptor downstream of the Tcrd promoter (TcrdGDL)<sup>19</sup> were treated with DT to deplete  $\gamma\delta$  T cells without affecting baseline cell shedding rates (Fig. S2). The number of LPS-induced shedding events was similar between DT- and vehicle-treated TcrdGDL mice, as well as DT-treated WT controls (Fig. 4C), confirming that despite the direct contact between  $\gamma\delta$  IELs and shedding cells,  $\gamma\delta$  T cells are not required for LPS-induced cell shedding.

CD103 is expressed by a variety of different immune cells in the intestinal mucosa, including IELs and intraepithelial innate lymphoid cells (ILC). However, the extent of LPS-induced CC3<sup>+</sup> shedding events was similar between Rag2/C $\gamma$  KO and WT mice (Fig. 4D). While these lymphocytes are not required for cell shedding to occur, our findings clearly indicate that both CD103 expression and the interactions between  $\gamma\delta$  IEL and shedding cells contribute to this process.

#### **The recognition of self- or stress ligands do not contribute to $\gamma\delta$ IEL-mediated LPS-induced cell shedding.**

We hypothesized that  $\gamma\delta$  IEL recognition of shedding cells via ligand-receptor interactions contributed to the recruitment of IELs to shedding enterocytes. Multiple studies have suggested that the  $\gamma\delta$  T cell receptor (TCR $\gamma\delta$ ) can recognize self-antigens, some of which may be upregulated by cell stress<sup>26</sup>; however, we found that TCR $\gamma\delta$  signaling is dispensable for LPS-induced apoptosis (Fig. S3A). Further, LPS treatment did not induce the expression of epithelial stress ligands recognized by NKG2D (Fig. S3B-D), and pre-treatment of mice with an anti-NKG2D blocking antibody failed to abrogate LPS-induced shedding (Fig. S3E). Thus, the mechanism by which  $\gamma\delta$  IELs recognize shedding cells remains an ongoing area of investigation.

#### **Granzymes mediate LPS-induced epithelial cell shedding.**

In addition to enabling ligand-binding interactions between IELs and epithelial cells, we posited that prolonged retention of IELs at sites of cell extrusion may also allow these cells to secrete a high local concentration of soluble proteins to facilitate shedding. Granzymes (Gzm) are a family of proteases with a wide range of targets that are highly expressed by NK cells, cytotoxic lymphocytes, and  $\gamma\delta$  IELs<sup>27, 28</sup>. In conjunction with perforin, a pore-forming protein that facilitates granzyme entry into target cells, granzymes initiate intracellular signaling cascades to induce apoptosis<sup>29</sup>. Moreover,

signaling through CD103 has been shown to promote degranulation of cytotoxic lymphocytes, resulting in the local polarized release of granzymes<sup>30, 31</sup>. To investigate the requirement for granzyme expression in LPS-induced shedding, lethally-irradiated Tcrd KO mice were engrafted with WT or GzmA/B-deficient bone marrow, thus generating bone marrow chimeras in which all hematopoietic cells are GzmA- and B-deficient. The initial irradiation of these mice did not affect baseline shedding rates (data not shown), and the resultant chimeras exhibited similar proportions of  $\gamma\delta$  and  $\alpha\beta$  IELs, regardless of the donor genotype (Fig. S4A). Following LPS treatment, mice engrafted with GzmA/B-deficient bone marrow exhibited a 31% decrease in CC3<sup>+</sup> enterocytes compared to WT, suggesting a role for at least one of these granzymes in mediating LPS-induced apoptotic cell shedding (Fig. 5A).

To examine the roles of individual granzymes in LPS-induced cell shedding, bone marrow chimeras were made engrafting Tcrd KO mice with WT, GzmA-, GzmB-, or GzmK-deficient bone marrow. While GzmK-deficient bone marrow chimeras did not exhibit significant differences compared to WT-engrafted mice, GzmA- or GzmB-deficient chimeras displayed 62% and 55% reductions in LPS-induced CC3<sup>+</sup> cells, respectively (Fig. 5B), indicating that GzmA and B both contribute to the extrusion of apoptotic enterocytes.

Both of these granzymes have been implicated in stimulating TNF production downstream of LPS-induced TLR4 activation<sup>32, 33</sup>. To test whether this phenomenon was responsible for the reduction in LPS-induced apoptosis observed in GzmA/B KO bone marrow chimeras, we treated GzmA/B-deficient mice with high-dose TNF. We found that GzmA/B KO mice exhibit a 47% decrease in CC3<sup>+</sup> cells in response to TNF (Fig. 5C), indicating that the observed reduction in apoptosis was not solely due to granzymes promoting TNF production in response to LPS. Next, using mixed bone marrow chimeras (80% Tcrd KO, 20% WT or GzmA/B KO) we showed that loss of  $\gamma\delta$  T-cell-derived GzmA and B results in a decrease in LPS-induced apoptosis in the jejunum as determined by CC3 staining (Fig. 5D, S4B). We did not observe an increase in TUNEL<sup>+</sup> cells in the epithelium of these chimeras, indicating that LPS was not inducing apoptosis in a CC3-independent manner in Gzm-deficient chimeras (Fig. S4C). Similar to CD103-deficient mice, we find that GzmA/B KO mice also exhibited a reduction in CC3<sup>+</sup> cells in the ileum (Fig. S4D), and the lack of propidium iodide labeling of shedding enterocytes confirmed that LPS treatment did not promote alternative cell death processes in these mice (Fig. S4E).

Based on the requirement for GzmA and B in LPS-induced cell shedding, we next asked whether  $\gamma\delta$  IELs directly induce epithelial apoptosis through a perforin-dependent mechanism. The frequency of CC3<sup>+</sup> shedding events in LPS-treated perforin-deficient mice (Prf1 KO) was similar to those observed in WT mice (Fig. 5E). Together, these data

indicate that GzmA and B promote LPS-induced shedding and apoptosis through a pathway independent of perforin-mediated intracellular enzymatic activity.

### **CD103 ligation promotes $\gamma\delta$ IEL granzyme release.**

Having demonstrated that GzmA and B facilitate LPS-induced cell shedding and given that these enzymes are among the most highly expressed proteins in  $\gamma\delta$  IELs at steady-state<sup>28, 34</sup>, we hypothesized that  $\gamma\delta$  IELs participate in the extrusion of apoptotic cells via extracellular granzyme release. Thus, to investigate the mechanisms by which  $\gamma\delta$  IELs secrete granzymes, we first assessed GzmA and B release by untreated, sort-purified WT  $\gamma\delta$  IELs. We were surprised to find that both GzmA and B are constitutively secreted by  $\gamma\delta$  IELs, with GzmA released to a greater extent than GzmB (375 pg vs. 1.5 pg/ $10^5$  cells). Since CD103/E-cadherin binding has been shown to promote degranulation of cytotoxic lymphocytes<sup>30, 35</sup>, we asked whether this interaction could promote granzyme secretion by stimulating  $\gamma\delta$  IELs with E-cadherin-Fc (E-cad-Fc). Notably, E-cad-Fc induced granzyme secretion, albeit to a lesser extent than anti-CD3 (Fig. 6A,B). Whereas anti-CD3 treatment resulted in substantial granzyme release via degranulation, as indicated by externalization of LAMP1 (CD107a), LAMP1 surface expression was not observed following E-cad-Fc stimulation (Fig. 6C). Consistent with this, immunofluorescence microscopy of  $\gamma\delta$  IELs revealed a subset of GzmA- or GzmB-containing vesicles that did not co-localize with LAMP1 (Fig. 6D,E). Taken together, this data indicates that  $\gamma\delta$  IELs secrete GzmA and B constitutively at steady-state and following CD103 engagement, which further potentiates granzyme release through LAMP1<sup>-</sup> secretory vesicles.

We next asked whether CD103 and GzmA/B contribute to the extrusion of apoptotic enterocytes in response to LPS through the same pathway. We found that blocking CD103 engagement does not further reduce the extent of LPS-induced apoptotic cell shedding in GzmA/B-deficient mice (Fig. 6F), thus supporting a model in which granzyme release occurs downstream of CD103/E-cadherin ligation to facilitate cell extrusion.

### **$\gamma\delta$ IELs associate with apoptotic enterocytes in Crohn's disease**

To examine whether  $\gamma\delta$  IELs are associated with apoptotic enterocytes in CD, we performed dual TCR $\gamma\delta$  and CC3 staining in biopsy sections obtained from control patients and those with active or quiescent CD (Fig. 7A, Supplementary Tables 1,2). While there was a significant increase in the association of  $\gamma\delta$  IELs with CC3<sup>+</sup> enterocytes in the duodenum

of patients with active or quiescent disease,  $\gamma\delta$  IELs were more often observed in association with CC3<sup>+</sup> cells in patients with inactive ileal disease (Fig. 7B,C). This finding may reflect the overall reduction in  $\gamma\delta$  IEL number in patients with active ileal CD<sup>36</sup>. We measured CC3 intensity around all IELs, yet found no association between control and CD patients, supporting our hypothesis that  $\gamma\delta$  IELs are associated with apoptosis in CD (Fig S5). Next, we mined a previously published scRNAseq dataset of IELs in CD<sup>36</sup> and found that CD103 (ITGAE) and GZMB expression are relatively unchanged, whereas GZMA expression is increased in  $\gamma\delta$  IELs isolated from surgical resections ( $P < 0.0001$ , Fig. 7D). Taken together, these data demonstrate that  $\gamma\delta$  IELs associate with apoptotic enterocytes in IBD patients, consistent with our observations in TNF-induced apoptosis in mice.

Journal Pre-proof

## Discussion

We now describe a novel role for  $\gamma\delta$  IELs in facilitating TNF-mediated shedding of apoptotic enterocytes. Our findings show that  $\gamma\delta$  IELs exhibit prolonged contact with apoptotic epithelial cells prior to their extrusion and that genetic or antibody-mediated inhibition of CD103/E-cadherin interactions abrogate apoptotic cell shedding in response to LPS. Further, loss of CD103 expression significantly reduces the frequency of CC3<sup>+</sup> shedding events and CD103 ligation promotes the constitutive secretion of extracellular GzmA and B by  $\gamma\delta$  IELs. Taken together, our data suggest that CD103 ligation functions to prolong  $\gamma\delta$  IEL contact with enterocytes and promote granzyme secretion, allowing the IEL to facilitate the shedding of apoptotic cells.

Although Lau et al. showed that Rag1- and Tcrd/Tcrb-knockout mice are both more susceptible to TNF-induced apoptosis<sup>25</sup>, we find that depletion of  $\gamma\delta$  IELs does not affect the extent of apoptotic cell shedding in response to LPS. This suggests that the presence of  $\alpha\beta$  T cells may be sufficient to inhibit this increase in TNF-induced apoptosis<sup>25</sup>. While multiple mechanisms may be involved in promoting TNFR-mediated apoptosis, our findings that (1) epithelial cells extrude more rapidly in LPS-treated  $\gamma\delta$  T-cell-deficient mice and (2) those apoptotic enterocytes that interact with  $\gamma\delta$  IELs are extruded from the epithelium more slowly than those that do not, suggests a potential subdivision of apoptotic cell shedding that has yet to be described. We posit that apoptotic enterocytes that do not receive a strong extrusion signal may secrete an as-yet-unidentified factor to recruit a  $\gamma\delta$  IEL to facilitate the shedding process.

Given the cytolytic capacity of  $\gamma\delta$  IELs<sup>11</sup>, we investigated potential mechanisms by which  $\gamma\delta$  IELs may recognize shedding enterocytes. Although IELs sense and kill infected or stressed enterocytes via activation of the TCR or recognition of stress ligands by NKG2D<sup>37,38</sup>, blocking either receptor had no effect on the number of CC3<sup>+</sup> shedding events. This was not surprising since changes in IEL surveillance behavior in response to bacterial invasion are TCR-independent<sup>39</sup>. As discussed above, it is likely that a chemokine or alternative stress ligand may be involved in crosstalk between  $\gamma\delta$  IELs and enterocytes in the early stages of apoptosis, which remains an interesting question for future investigation.

Previous work from our laboratory has demonstrated that both ligand-receptor interactions and cytokine signaling influence the dynamics of  $\gamma\delta$  IEL motility<sup>14,15,22</sup>. Although largely presumed to function as a gut homing and retention signal, the biological consequences of CD103 ligation by E-cadherin remain unclear. In the context of cell migration, CD103/E-cadherin interactions influence lymphocyte morphology and motility<sup>40</sup>, and deletion of CD103 reduces  $\gamma\delta$  IEL

retention in the LIS, thus increasing the patrolling behavior of these cells to limit bacterial invasion<sup>15</sup>. We hypothesize that CD103 ligation may result in short calcium transients that function as a stop signal to temporarily arrest  $\gamma\delta$  IEL motility in a manner similar to TCR-mediated 'search' behavior<sup>41</sup>. We now show CD103 functions to retain  $\gamma\delta$  IELs at sites of cell shedding, and CD103 ligation by E-cadherin is sufficient to stimulate granzyme secretion in the absence of TCR signaling. This finding is consistent with a previous study showing that engagement of CD103 with E-cad-Fc induces granule polarization and granzyme release by CTLs<sup>30</sup>. However, the lack of LAMP1 externalization upon E-cad-Fc-stimulated granzyme release by  $\gamma\delta$  IELs reveals an alternative pathway for granzyme secretion, one that is reminiscent of the constitutive release of newly-synthesized granzymes by activated CTLs<sup>42</sup>. Together, these data demonstrate a dual role for CD103 in (1) mediating extended contact between  $\gamma\delta$  IELs and shedding enterocytes, and (2) directly stimulating granzyme release through engagement of epithelial E-cadherin, ultimately resulting in the enhanced local deposition of granzymes to facilitate cell shedding.

Granzymes A and B, but not perforin, contributed to LPS-induced shedding of apoptotic cells, thus providing strong evidence that  $\gamma\delta$  IELs facilitate cell shedding through a mechanism other than direct lysis. Extracellular granzymes have been shown to promote the proteolytic cleavage of ECM proteins such as type IV collagen (GzmA), fibronectin (GzmA/B), and laminin (GzmB), which are found in the intestinal BM<sup>43-46</sup>. Extracellular GzmB was also recently shown to cleave  $\alpha_6$  integrin, a component of the hemidesmosome that is critical in anchoring epithelial cells to the BM<sup>47</sup>. Moreover, circulating lymphocytes have been shown to secrete GzmA and B to remodel the vascular BM and facilitate extravasation<sup>43, 48</sup>. These reports lead us to hypothesize that  $\gamma\delta$  IELs promote cell extrusion by remodeling the BM beneath cells that have initiated the shedding process. Given the role of GzmA and B in promoting lymphocyte migration, future studies will investigate the possibility that granzymes contribute to cell shedding by facilitating  $\gamma\delta$  IEL motility.

Lastly, we show an increased interaction between  $\gamma\delta$  IELs and CC3<sup>+</sup> cells in patients with either active or quiescent CD, none of whom had a record of anti-TNF therapy. The association between pathological cell shedding and CD relapse<sup>8</sup> coupled with the involvement of CD103 in this process highlight a potential benefit for CD103 blockade in IBD therapy. Vedolizumab has been shown to induce and sustain disease remission by blocking  $\alpha_4\beta_7$  integrin, thus inhibiting the entry of lymphocytes into the gut<sup>49, 50</sup>. However, the effect of this drug on tissue-resident lymphocyte migratory behavior remains unknown. Etrolizumab, which targets the  $\beta_7$  subunit of both  $\alpha_4\beta_7$  and  $\alpha_E\beta_7$  (CD103) integrins, is currently in phase III clinical trials for CD<sup>51</sup>. Given our studies implicating CD103 in TNF-induced cell shedding, a

pan- $\beta_7$  inhibitor may provide the additional benefits of regulating IEL motility and limiting shedding events. Thus, our findings strengthen the therapeutic potential of targeting CD103 and suggest that this may be a viable approach to control cell shedding via modulation of  $\gamma\delta$  IEL behavior in CD patients in remission, with an ultimate goal of maintaining homeostasis and preventing relapse.

Journal Pre-proof

**Figure Legends.****Figure 1.  $\gamma\delta$  IELs directly interact with shedding enterocytes.**

(A) Immunostaining and (B) quantification of cleaved caspase-3 (CC3)<sup>+</sup> shedding events in the jejunum of PBS- or LPS-treated WT mice (red asterisks). Scale bar=50 $\mu$ m. BM, basement membrane. (C) Representative transmission electron micrographs of PBS- and LPS-treated WT jejunum. IELs are pseudocolored blue. SC, shedding cell. Scale bar = 2.5 $\mu$ m (D) Immunofluorescent micrograph of  $\gamma\delta$  IELs (white) interacting with CC3<sup>+</sup> shedding cells (magenta). Green: ZO-1; blue: nuclei. Asterisks indicate shedding cells. Scale bar=5 $\mu$ m. n=3-8 mice per condition; \*\*\**P* < .001.

**Figure 2.  $\gamma\delta$  IELs maintain prolonged contact with enterocytes prior to extrusion into the lumen.**

Intravital microscopy of (A) TcrdEGFP or (D) TcrdGDL mRFP-ZO1 mice treated with LPS. (A) Time-lapse images from intravital imaging show  $\gamma\delta$  IELs (green) interacting with multiple shedding cells (asterisks). Red: lumen; white: nuclei. Scale bar=20 $\mu$ m. (B) Mean track speed of  $\gamma\delta$  IELs that are or are not associated with shedding cells. (C) Dwell time of  $\gamma\delta$  IELs at sites of shedding or within the LIS. (D)  $\gamma\delta$  IEL (green) interacting with a ZO-1 funnel (F, white). TJ: tight junction; EC: extruding cell. Scale bar=5 $\mu$ m. n=6-8 mice; \**P* < .05, \*\*\**P* < .001.

**Figure 3. Deletion or antibody-mediated blockade of CD103 abrogates pathological cell shedding.**

Representative immunostaining and quantification of CC3<sup>+</sup> epithelial cells in WT or CD103 KO mice treated with (A,B) LPS or (C) TNF. Asterisks: shedding cells. Scale bar=50 $\mu$ m. (D) Percent of shedding cells contacted by a  $\gamma\delta$  IEL and (E)  $\gamma\delta$  IEL dwell time near shedding cells in LPS-treated WT or CD103 KO mice. (F) Quantification of CC3<sup>+</sup> cells in the jejunum of WT mice treated with anti-CD103 or isotype control prior to LPS administration. n=3-9 mice (9-26 tracks); \**P* < .05, \*\**P* < .01, #*P* < .0001.

**Figure 4.  $\gamma\delta$  IELs are not required for LPS-induced cell shedding.**

Quantification of (A) CC3<sup>+</sup> cells in jejunal tissue of WT or Tcrd KO mice treated with LPS. (B) Track speed of extruding enterocyte in LPS-treated WT (with or without  $\gamma\delta$  IEL contact) or Tcrd KO mice. (C) WT or TcrdGDL mice were treated with diphtheria toxin (DT) or vehicle control prior to LPS treatment. (D) WT or Rag2/C $\gamma$  KO mice were treated with PBS or LPS. n=2-8 mice; \**P* < .05, n.s., not significant.

**Figure 5. Granzymes A and B mediate LPS-induced epithelial cell shedding in a perforin-independent manner.**

Quantification of CC3<sup>+</sup> shedding events in jejunal tissue. Lethally irradiated Tcrd-deficient mice were engrafted with (A) GzmA/B KO or (B) WT, GzmA KO, GzmB KO, GzmK KO and treated with LPS. (C) GzmA/B KO or WT mice treated with TNF. (D) LPS-treated WT or GzmA/B KO mixed bone marrow chimeras. (E) WT or Prf1 KO mice treated with PBS or LPS. n=3-14 mice; n.s., not significant \**P* < .05, \*\**P* < .01.

**Figure 6. CD103 ligation promotes degranulation-independent granzyme release by  $\gamma\delta$  IELs.**

WT or CD103 KO  $\gamma\delta$  IELs were stimulated with E-cad-Fc or anti-CD3 and ELISA performed on cell supernatants for (A) GzmA and (B) GzmB. Fold change compared to untreated WT  $\gamma\delta$  IELs. (C) Frequency of LAMP1 externalization in  $\gamma\delta$  IELs under the same conditions. (D) Immunofluorescence micrographs (left) and 3D reconstructions of WT  $\gamma\delta$  IELs showing LAMP1 (magenta), GzmA or B (cyan). Gzm-containing LAMP1<sup>+</sup> and LAMP1<sup>-</sup> vesicles are shown in yellow and cyan, respectively. Scale bar = 2 $\mu$ m. (E) Co-localization of LAMP1 and GzmA or B. (F) Quantification of CC3<sup>+</sup> shedding cells in LPS-treated GzmA/B KO mice pre-treated with IgG or anti-CD103. Dashed line indicates representative amount of shedding observed in LPS-treated WT mice. n.s., not significant \**P* < .05, \*\**P* < .01.

**Figure 7.  $\gamma\delta$  IELs are in close proximity to shedding apoptotic enterocytes in Crohn's disease biopsies.**

(A) Representative immunostaining of  $\gamma\delta$ TCR (brown) and CC3 (blue) in sections from normal and active CD duodenal biopsies. Scale bar = 50 $\mu$ m. Quantification of CC3-associated  $\gamma\delta$  T cells in tissue sections of (B) duodenal and (C) ileal biopsies with normal histology, quiescent or active CD. (D) Violin plots showing ITGAE, GZMA and GZMB expression in  $\gamma\delta$  IELs in control and CD samples. n=4-9 patients. n.s., not significant \**P* < .05, \*\**P* < .01.

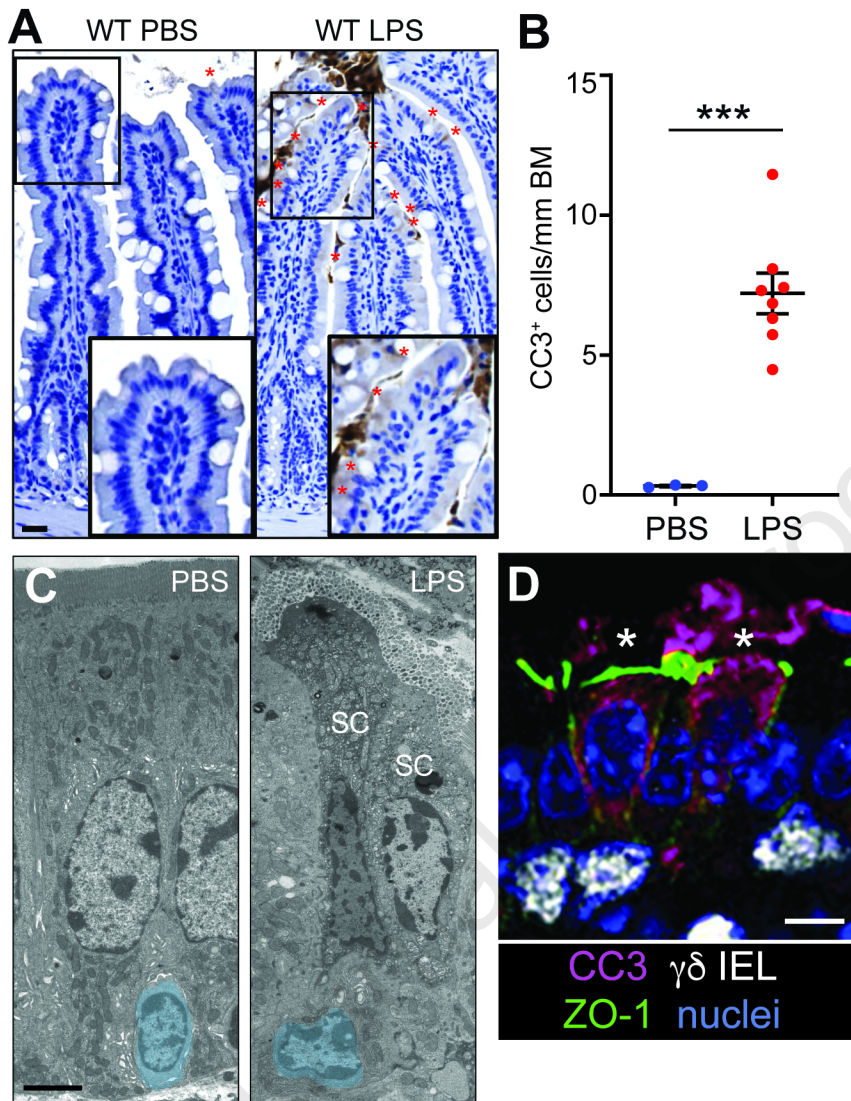
## References

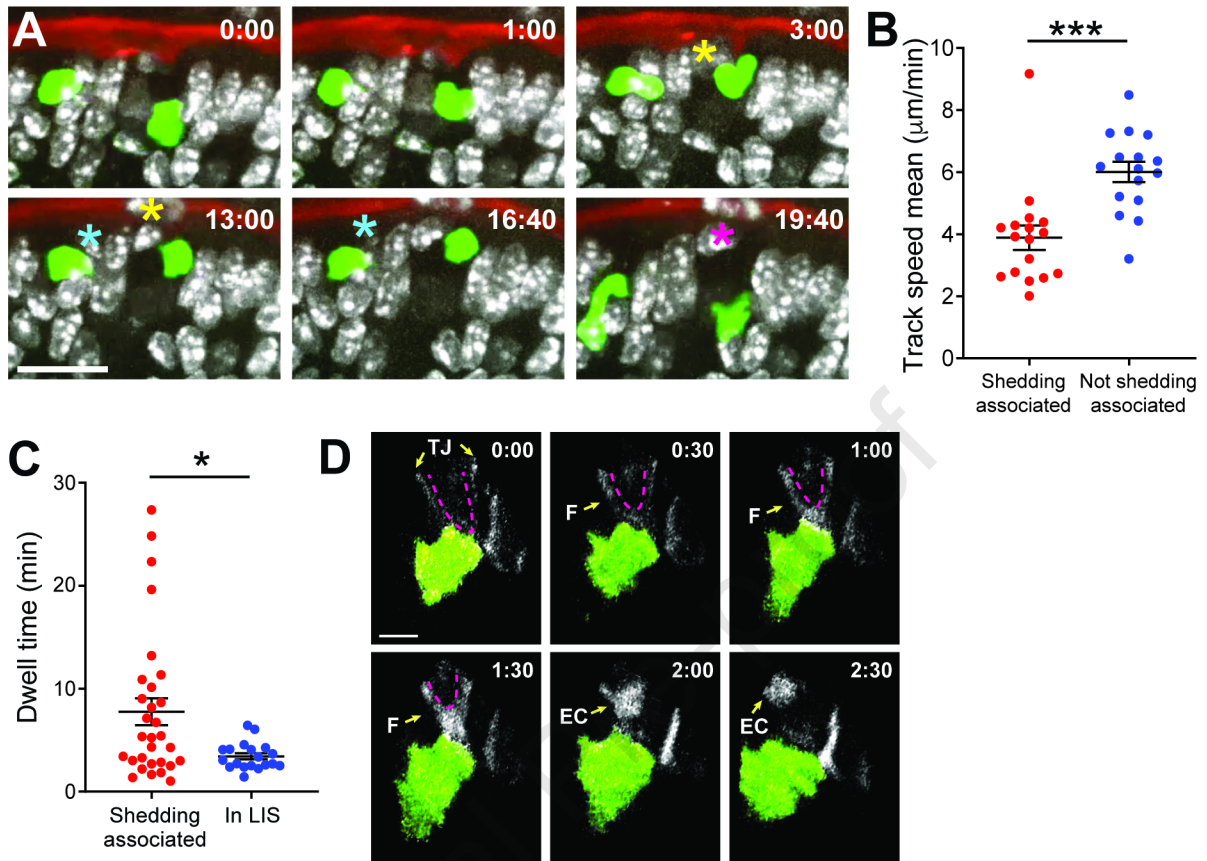
1. France MM, Turner JR. The mucosal barrier at a glance. *J Cell Sci* 2017;130:307-314.
2. Parker A, Vaux L, Patterson AM, et al. Elevated apoptosis impairs epithelial cell turnover and shortens villi in TNF-driven intestinal inflammation. *Cell Death Dis* 2019;10:108.
3. Di Sabatino A, Ciccocioppo R, Luinetti O, et al. Increased enterocyte apoptosis in inflamed areas of Crohn's disease. *Dis Colon Rectum* 2003;46:1498-507.
4. Hagiwara C, Tanaka M, Kudo H. Increase in colorectal epithelial apoptotic cells in patients with ulcerative colitis ultimately requiring surgery. *J Gastroenterol Hepatol* 2002;17:758-64.
5. Collaborators GBDIBD. The global, regional, and national burden of inflammatory bowel disease in 195 countries and territories, 1990-2017: a systematic analysis for the Global Burden of Disease Study 2017. *Lancet Gastroenterol Hepatol* 2020;5:17-30.
6. Breese EJ, Michie CA, Nicholls SW, et al. Tumor necrosis factor alpha-producing cells in the intestinal mucosa of children with inflammatory bowel disease. *Gastroenterology* 1994;106:1455-66.
7. Baert FJ, D'Haens GR, Peeters M, et al. Tumor necrosis factor alpha antibody (infliximab) therapy profoundly down-regulates the inflammation in Crohn's ileocolitis. *Gastroenterology* 1999;116:22-8.
8. Kiesslich R, Duckworth CA, Moussata D, et al. Local barrier dysfunction identified by confocal laser endomicroscopy predicts relapse in inflammatory bowel disease. *Gut* 2012;61:1146-53.
9. Williams JM, Duckworth CA, Watson AJ, et al. A mouse model of pathological small intestinal epithelial cell apoptosis and shedding induced by systemic administration of lipopolysaccharide. *Dis Model Mech* 2013;6:1388-99.
10. Marchiando AM, Shen L, Graham WV, et al. The epithelial barrier is maintained by in vivo tight junction expansion during pathologic intestinal epithelial shedding. *Gastroenterology* 2011;140:1208-1218 e1-2.
11. Hu MD, Jia L, Edelblum KL. Policing the intestinal epithelial barrier: Innate immune functions of intraepithelial lymphocytes. *Curr Pathobiol Rep* 2018;6:35-46.
12. Komano H, Fujiura Y, Kawaguchi M, et al. Homeostatic regulation of intestinal epithelia by intraepithelial gamma delta T cells. *Proc Natl Acad Sci U S A* 1995;92:6147-51.
13. Chen Y, Chou K, Fuchs E, et al. Protection of the intestinal mucosa by intraepithelial gamma delta T cells. *Proc Natl Acad Sci U S A* 2002;99:14338-43.
14. Edelblum KL, Shen L, Weber CR, et al. Dynamic migration of gammadelta intraepithelial lymphocytes requires occludin. *Proc Natl Acad Sci U S A* 2012;109:7097-102.
15. Edelblum KL, Singh G, Odenwald MA, et al. gammadelta Intraepithelial Lymphocyte Migration Limits Transepithelial Pathogen Invasion and Systemic Disease in Mice. *Gastroenterology* 2015;148:1417-26.
16. Itohara S, Mombaerts P, Lafaille J, et al. T cell receptor delta gene mutant mice: independent generation of alpha beta T cells and programmed rearrangements of gamma delta TCR genes. *Cell* 1993;72:337-48.
17. Prinz I, Sansoni A, Kissenpfennig A, et al. Visualization of the earliest steps of gammadelta T cell development in the adult thymus. *Nat Immunol* 2006;7:995-1003.
18. Marchiando AM, Shen L, Graham WV, et al. Caveolin-1-dependent occludin endocytosis is required for TNF-induced tight junction regulation in vivo. *J Cell Biol* 2010;189:111-26.

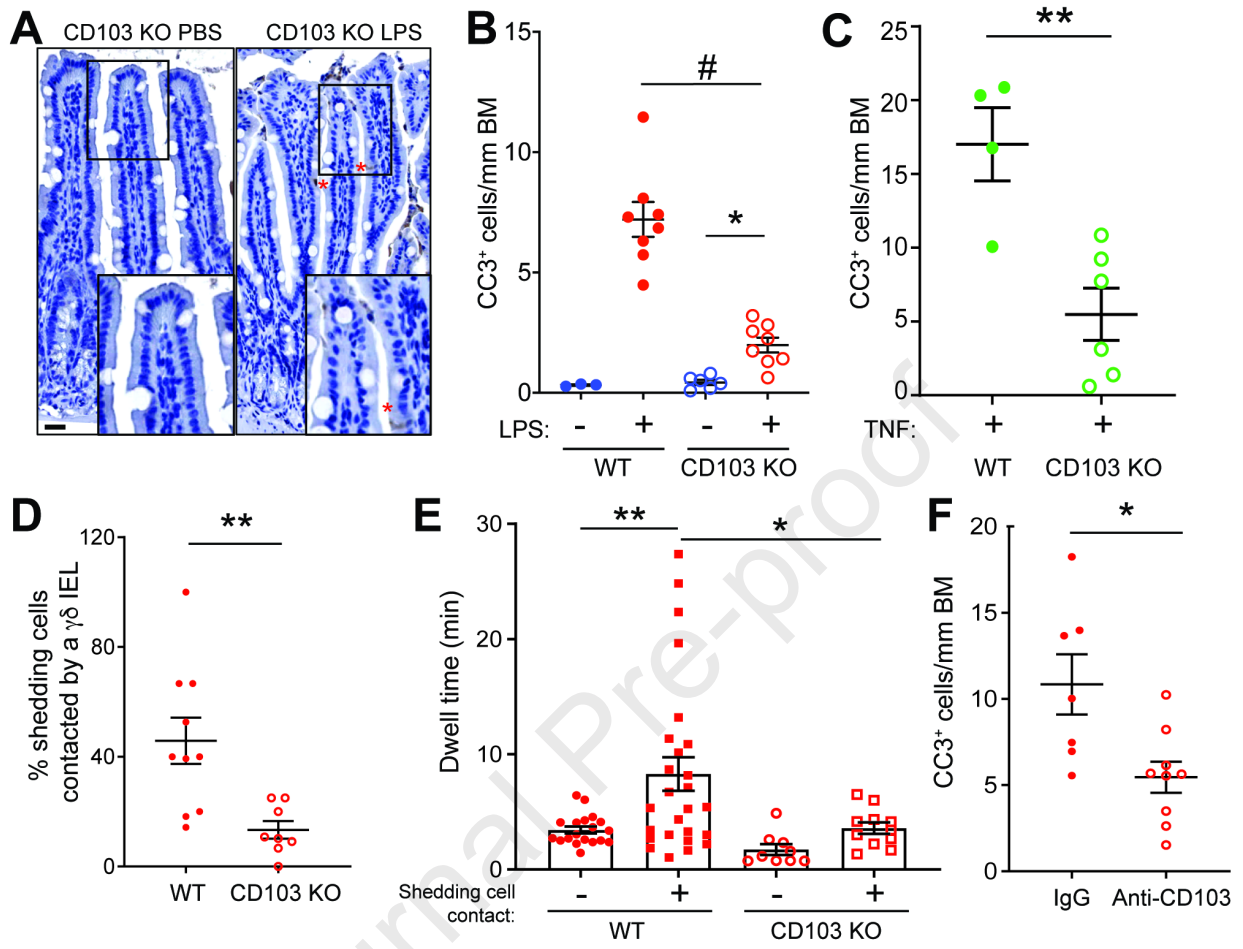
19. Sandrock I, Reinhardt A, Ravens S, et al. Genetic models reveal origin, persistence and non-redundant functions of IL-17-producing gammadelta T cells. *J Exp Med* 2018;215:3006-3018.
20. Rauch I, Deets KA, Ji DX, et al. NAIP-NLRC4 Inflammasomes Coordinate Intestinal Epithelial Cell Expulsion with Eicosanoid and IL-18 Release via Activation of Caspase-1 and -8. *Immunity* 2017;46:649-659.
21. Jia L, Edelblum KL. Intravital Imaging of Intraepithelial Lymphocytes in Murine Small Intestine. *J Vis Exp* 2019.
22. Hu MD, Ethridge AD, Lipstein R, et al. Epithelial IL-15 Is a Critical Regulator of gammadelta Intraepithelial Lymphocyte Motility within the Intestinal Mucosa. *J Immunol* 2018;201:747-756.
23. Shibahara T, Sato N, Waguri S, et al. The fate of effete epithelial cells at the villus tips of the human small intestine. *Arch Histol Cytol* 1995;58:205-19.
24. Schon MP, Arya A, Murphy EA, et al. Mucosal T lymphocyte numbers are selectively reduced in integrin alpha E (CD103)-deficient mice. *J Immunol* 1999;162:6641-9.
25. Lau KS, Cortez-Retamozo V, Philips SR, et al. Multi-scale in vivo systems analysis reveals the influence of immune cells on TNF-alpha-induced apoptosis in the intestinal epithelium. *PLoS Biol* 2012;10:e1001393.
26. Born WK, Kemal Aydintug M, O'Brien RL. Diversity of gammadelta T-cell antigens. *Cell Mol Immunol* 2013;10:13-20.
27. Chowdhury D, Lieberman J. Death by a thousand cuts: granzyme pathways of programmed cell death. *Annu Rev Immunol* 2008;26:389-420.
28. Shires J, Theodoridis E, Hayday AC. Biological insights into TCRgammadelta+ and TCRalphabeta+ intraepithelial lymphocytes provided by serial analysis of gene expression (SAGE). *Immunity* 2001;15:419-34.
29. Russell JH, Ley TJ. Lymphocyte-mediated cytotoxicity. *Annu Rev Immunol* 2002;20:323-70.
30. Le Floch A, Jalil A, Franciszkiewicz K, et al. Minimal engagement of CD103 on cytotoxic T lymphocytes with an E-cadherin-Fc molecule triggers lytic granule polarization via a phospholipase Cgamma-dependent pathway. *Cancer Res* 2011;71:328-38.
31. Franciszkiewicz K, Le Floch A, Boutet M, et al. CD103 or LFA-1 engagement at the immune synapse between cytotoxic T cells and tumor cells promotes maturation and regulates T-cell effector functions. *Cancer Res* 2013;73:617-28.
32. Wensink AC, Kemp V, Fermie J, et al. Granzyme K synergistically potentiates LPS-induced cytokine responses in human monocytes. *Proc Natl Acad Sci U S A* 2014;111:5974-9.
33. **Spencer CT, Abate G, Sakala IG**, et al. Granzyme A produced by gamma(9)delta(2) T cells induces human macrophages to inhibit growth of an intracellular pathogen. *PLoS Pathog* 2013;9:e1003119.
34. Fahrner AM, Konigshofer Y, Kerr EM, et al. Attributes of gammadelta intraepithelial lymphocytes as suggested by their transcriptional profile. *Proc Natl Acad Sci U S A* 2001;98:10261-6.
35. Smyth LJ, Kirby JA, Cunningham AC. Role of the mucosal integrin alpha(E)(CD103)beta(7) in tissue-restricted cytotoxicity. *Clin Exp Immunol* 2007;149:162-70.
36. Jaeger N, Gamini R, Cella M, et al. Single-cell analyses of Crohn's disease tissues reveal intestinal intraepithelial T cells heterogeneity and altered subset distributions. *Nat Commun* 2021;12:1921.
37. Wu J, Groh V, Spies T. T cell antigen receptor engagement and specificity in the recognition of stress-inducible MHC class I-related chains by human epithelial gamma delta T cells. *J Immunol* 2002;169:1236-40.

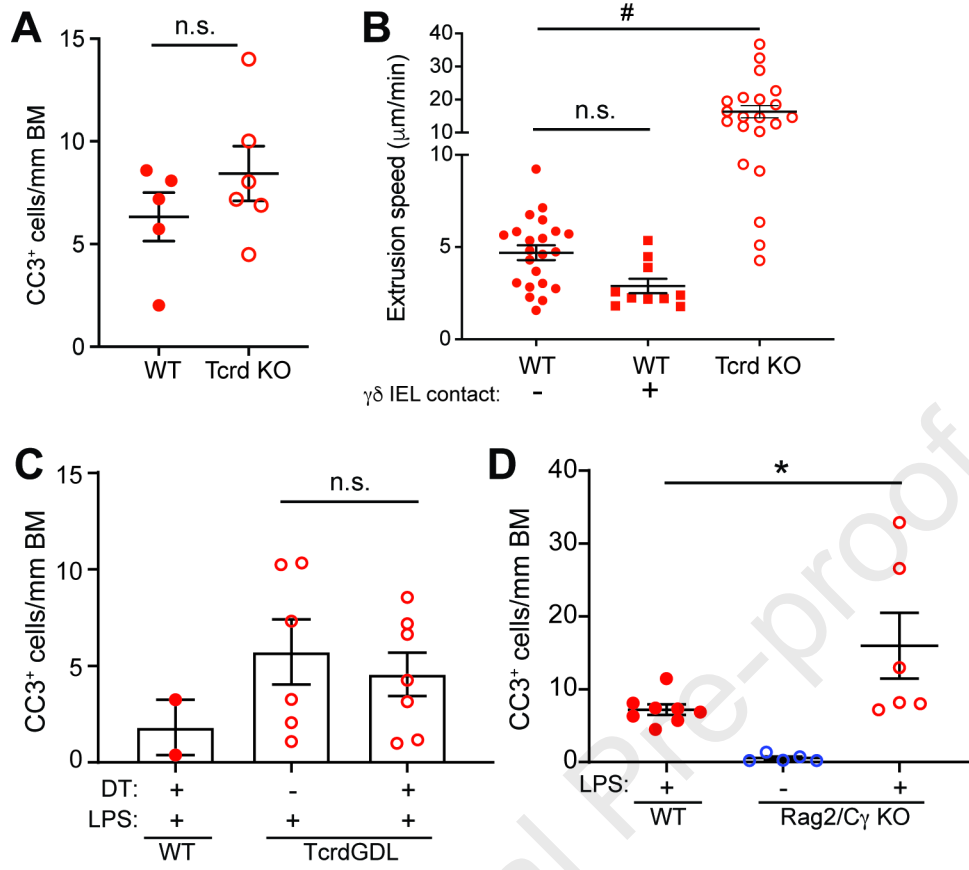
38. Li Z, Zhang C, Zhou Z, et al. Small intestinal intraepithelial lymphocytes expressing CD8 and T cell receptor gammadelta are involved in bacterial clearance during *Salmonella enterica* serovar Typhimurium infection. *Infect Immun* 2012;80:565-74.
39. **Hoytema van Konijnenburg DP, Reis BS**, Pedicord VA, et al. Intestinal Epithelial and Intraepithelial T Cell Crosstalk Mediates a Dynamic Response to Infection. *Cell* 2017;171:783-794.
40. Schlickum S, Sennefelder H, Friedrich M, et al. Integrin alpha E(CD103)beta 7 influences cellular shape and motility in a ligand-dependent fashion. *Blood* 2008;112:619-25.
41. Dustin ML, Bromley SK, Kan Z, et al. Antigen receptor engagement delivers a stop signal to migrating T lymphocytes. *Proc Natl Acad Sci U S A* 1997;94:3909-13.
42. Isaza S, Baetz K, Olsen K, et al. Serial killing by cytotoxic T lymphocytes: T cell receptor triggers degranulation, re-filling of the lytic granules and secretion of lytic proteins via a non-granule pathway. *Eur J Immunol* 1995;25:1071-9.
43. Simon MM, Kramer MD, Prester M, et al. Mouse T-cell associated serine proteinase 1 degrades collagen type IV: a structural basis for the migration of lymphocytes through vascular basement membranes. *Immunology* 1991;73:117-9.
44. Buzza MS, Zamurs L, Sun J, et al. Extracellular matrix remodeling by human granzyme B via cleavage of vitronectin, fibronectin, and laminin. *J Biol Chem* 2005;280:23549-58.
45. Froelich CJ, Zhang X, Turbov J, et al. Human granzyme B degrades aggrecan proteoglycan in matrix synthesized by chondrocytes. *J Immunol* 1993;151:7161-71.
46. Turner CT, Zeglinski MR, Richardson KC, et al. Granzyme B Contributes to Barrier Dysfunction in Oxazolone-Induced Skin Inflammation through E-Cadherin and FLG Cleavage. *J Invest Dermatol* 2021;141:36-47.
47. Hiroyasu S, Zeglinski MR, Zhao H, et al. Granzyme B inhibition reduces disease severity in autoimmune blistering diseases. *Nat Commun* 2021;12:302.
48. Prakash MD, Munoz MA, Jain R, et al. Granzyme B promotes cytotoxic lymphocyte transmigration via basement membrane remodeling. *Immunity* 2014;41:960-72.
49. Wyant T, Fedyk E, Abhyankar B. An Overview of the Mechanism of Action of the Monoclonal Antibody Vedolizumab. *J Crohns Colitis* 2016;10:1437-1444.
50. Lowenberg M, Vermeire S, Mostafavi N, et al. Vedolizumab Induces Endoscopic and Histologic Remission in Patients With Crohn's Disease. *Gastroenterology* 2019;157:997-1006 e6.
51. Vermeire S, O'Byrne S, Keir M, et al. Etrolizumab as induction therapy for ulcerative colitis: a randomised, controlled, phase 2 trial. *Lancet* 2014;384:309-18.

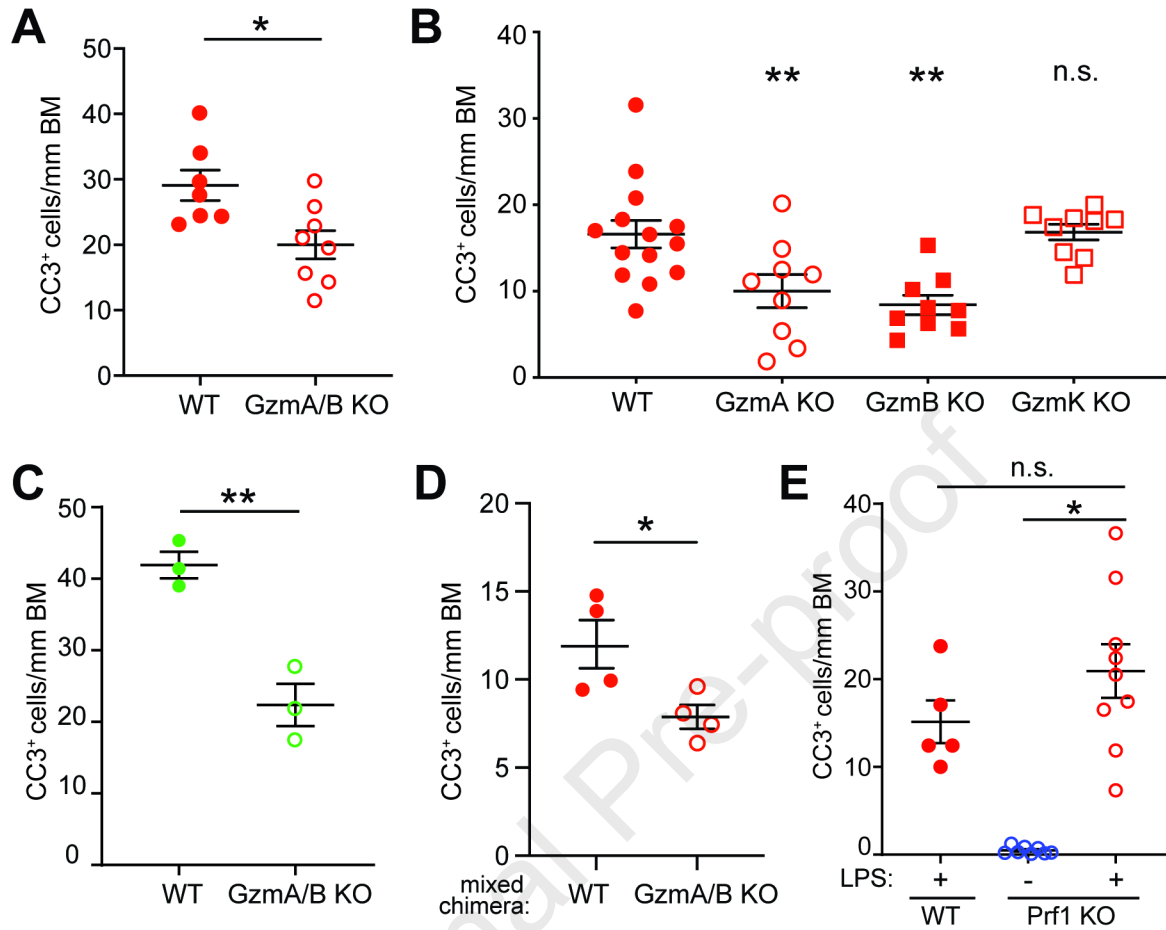
Author names in bold designate shared co-first authorship.

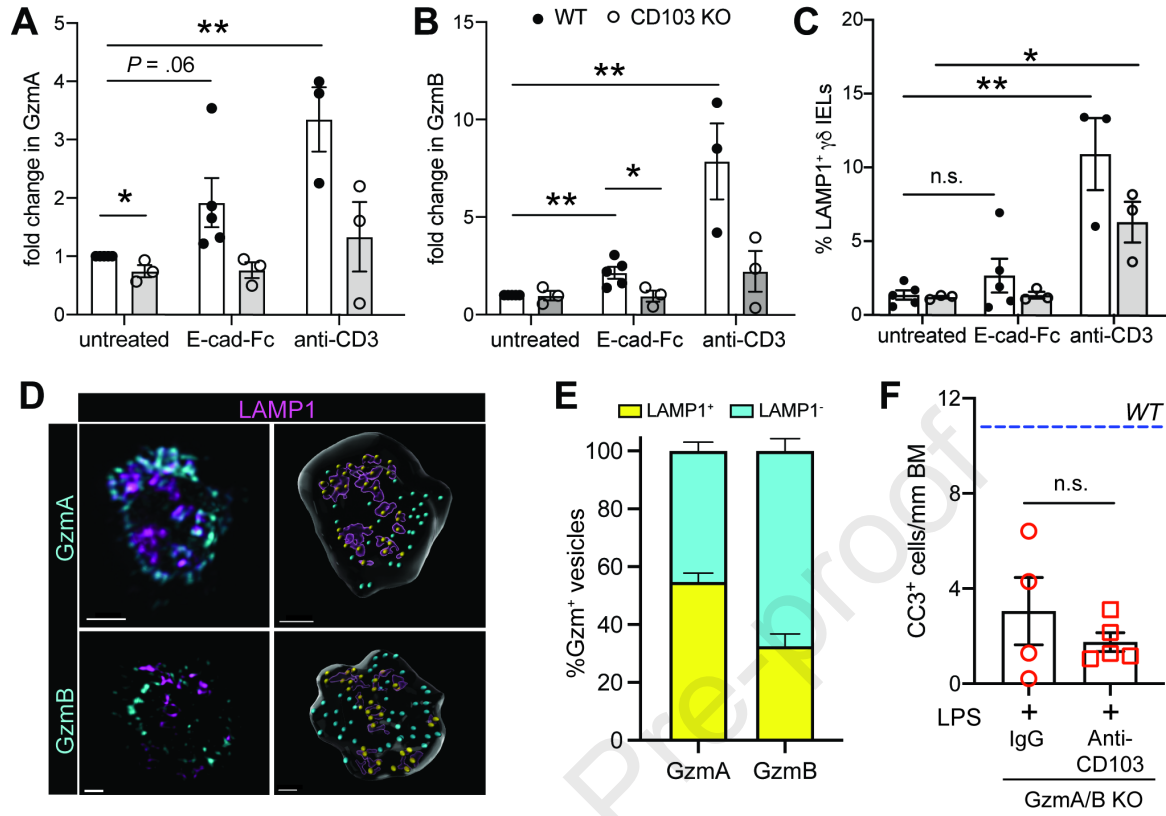


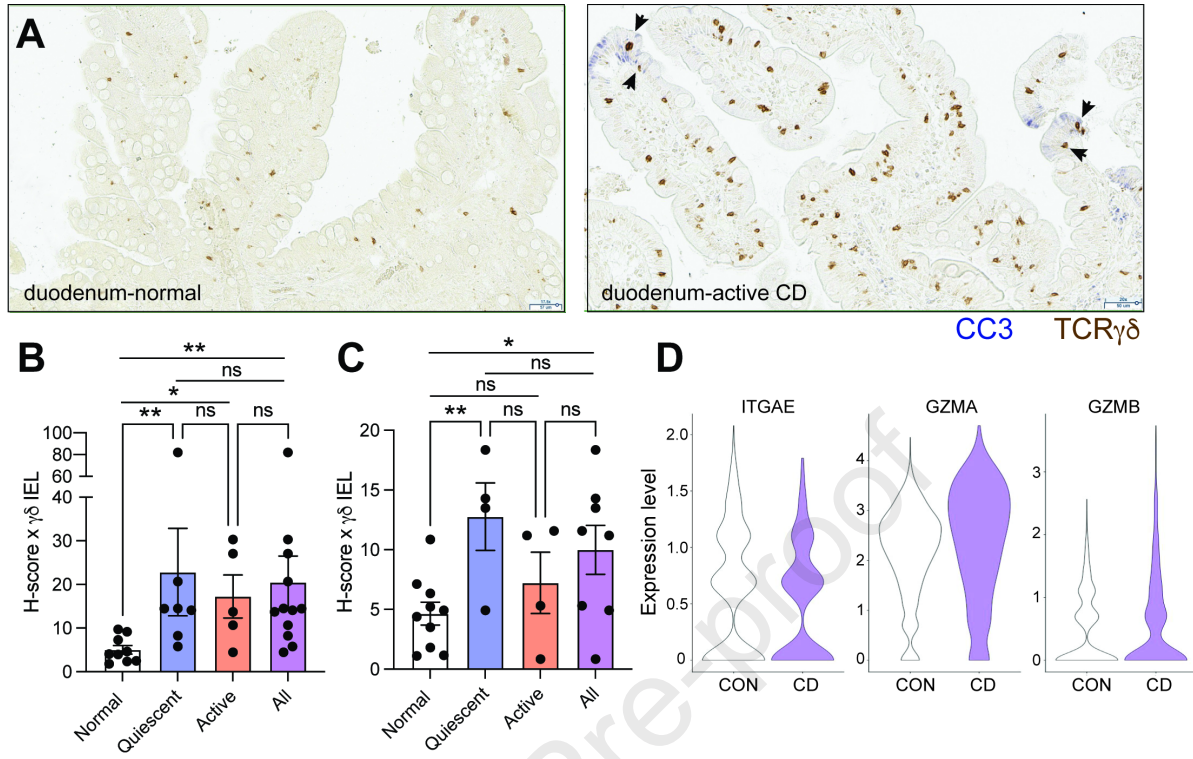


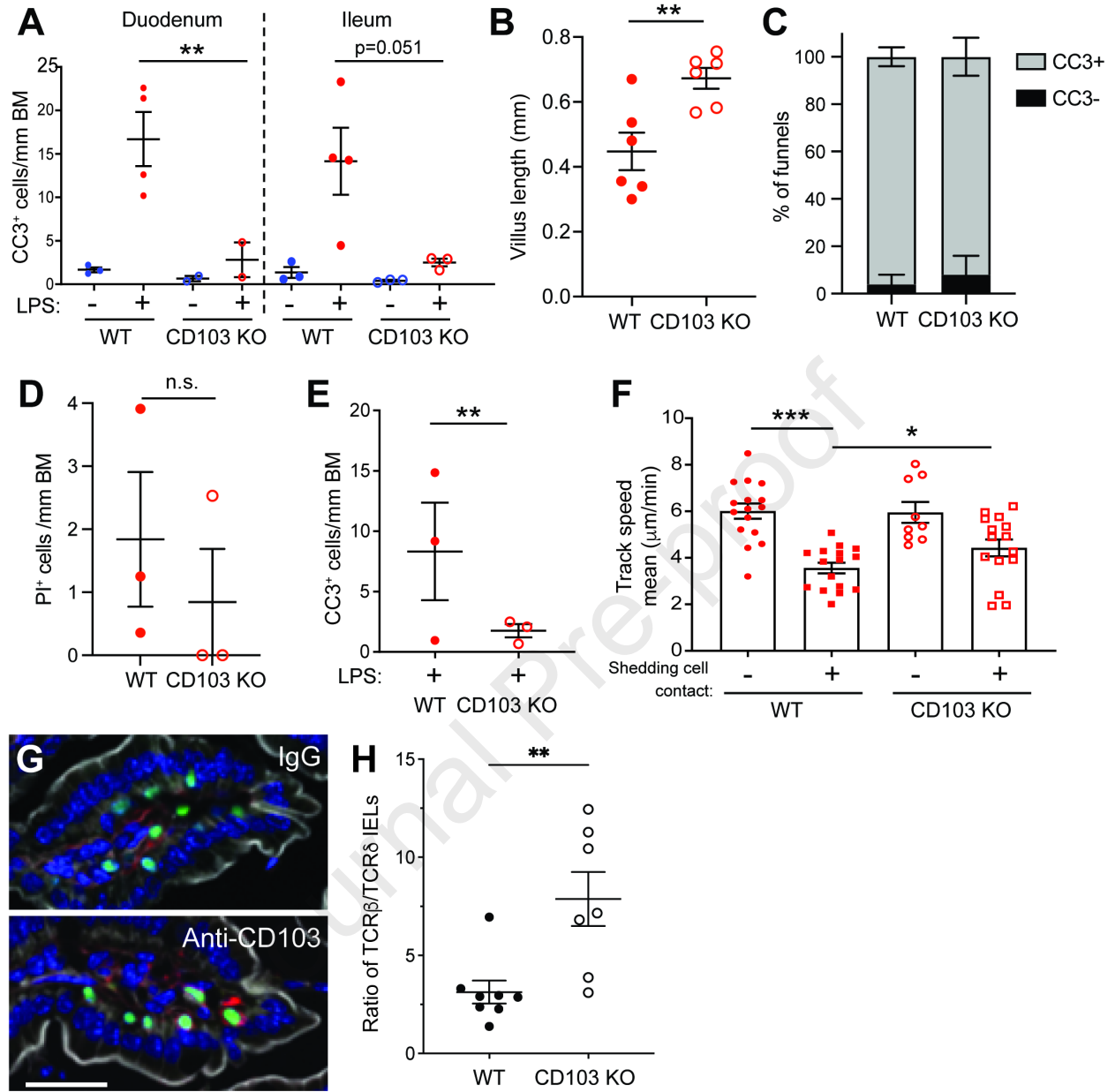


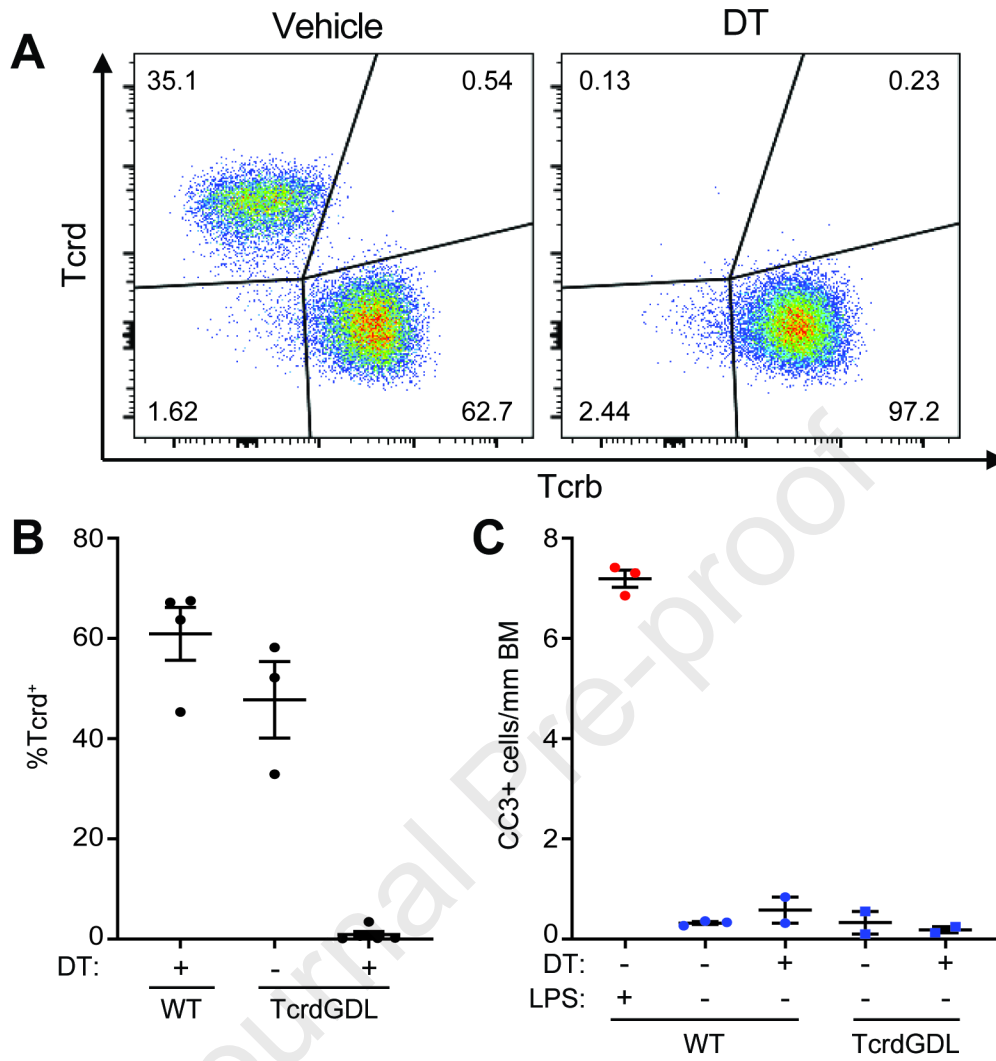


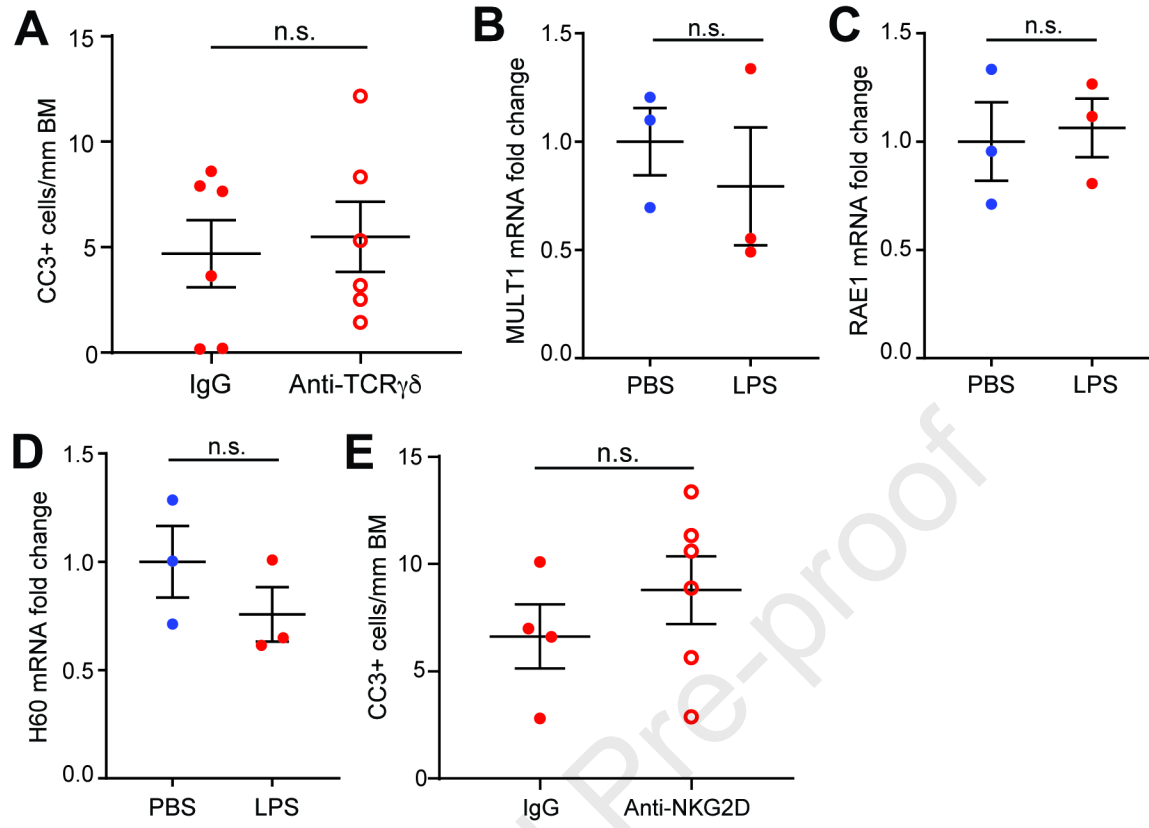


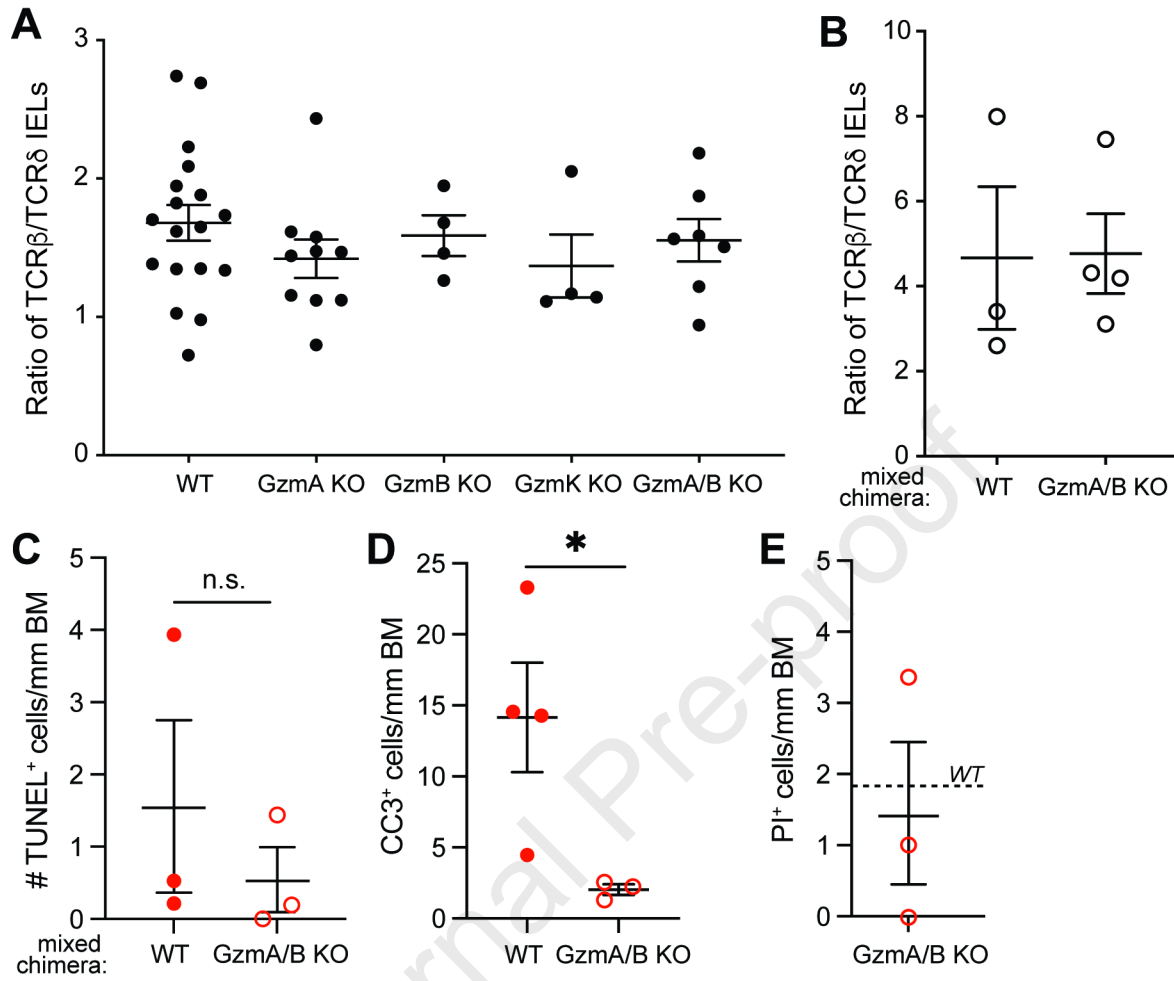




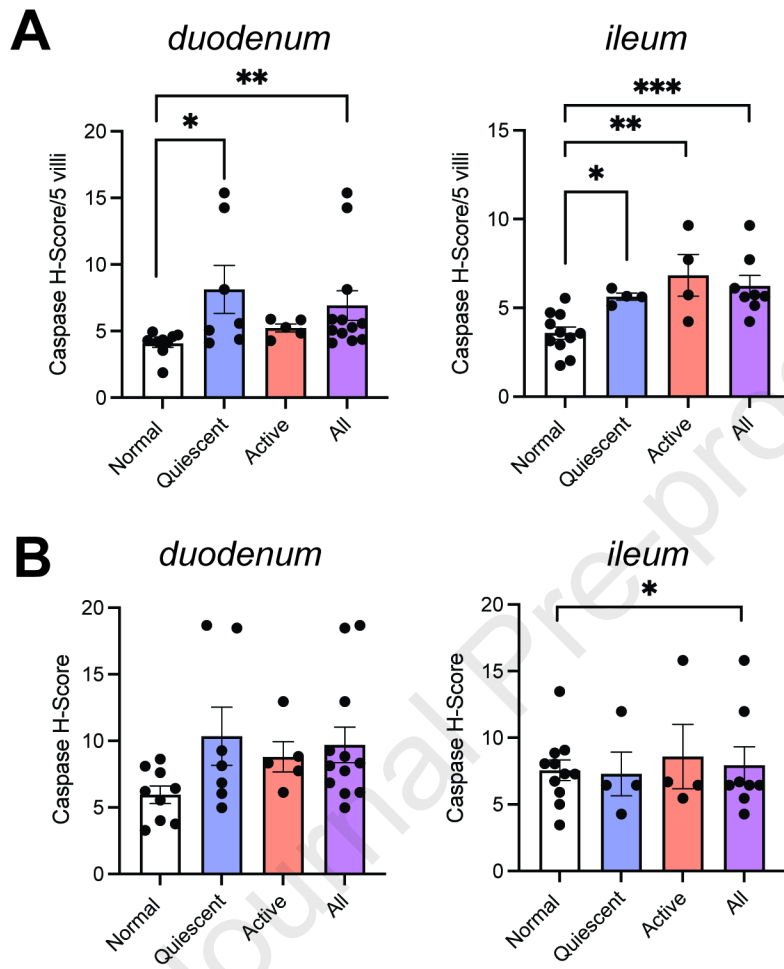








Supplementary Figure 5



Supplementary Table 1: Cohort characteristics for duodenal biopsies

	<b>Controls</b>	<b>Crohns</b>	<b><i>p</i> value</b>
	n=9	n=15	
Age (Years±SD)	38±21.11	34.87±14.42	0.7005
Female (%)	5 (55.56)	9 (60.00)	>0.9999
Duodenal inflammation evident (%)	n/a	8 (53.33)	-
Medications relevant to IBD (%)			
Levothyroxine	n/a	1 (6.67)	-
Azathioprine	n/a	3 (20.00)	-
Pantoprazole	n/a	2 (13.33)	-
Mesalamine	n/a	1 (6.67)	-

Supplementary Table 2: Cohort characteristics for ileal biopsies

	<b>Controls</b>	<b>Crohns</b>	<b><i>p</i> value</b>
	n=17	n=8	
Age (Years±SD)	49.82s±14.46	38.88s±21.96	0.2278
Female (%)	11 (64.71)	5 (62.50)	>0.9999
Ileal inflammation evident (%)	n/a	4 (50.00)	-

## **Supplementary Methods**

### **Immunofluorescent and immunohistochemical staining**

Frozen sections, 5  $\mu\text{m}$  thick, of fixed mouse intestine were obtained as previously described<sup>17</sup> and immunostained with Alexa Fluor 594-conjugated anti-Rat IgG, Alexa Fluor 647-conjugated phalloidin and Hoechst 33342 (Life Technologies, Waltham, MA). Slides were mounted with Prolong Glass (Life Technologies).

To visualize granzymes and vesicles within IELs, small intestinal IELs were isolated, sort-purified, fixed and permeabilized with Cytotfix/Cytoperm (BD Biosciences, Franklin Lakes, NJ) and stained with antibodies against Granzyme A, Granzyme B, LAMP1 (BioLegend, San Diego, CA). The appropriate secondary antibodies and Hoechst 33342 (Life Technologies) were applied, and the cells were affixed to glass slides by cytocentrifugation and mounted in Prolong Glass (Life Technologies). Co-localization was determined by generating surfaces for LAMP1 and spots for Gzm<sup>+</sup> vesicles using Imaris (v. 9.7.1; Bitplane, South Windsor, CT). Surfaces were generated to demarcate individual cells for vesicle classification. The distance between Gzm spots (0.35 $\mu\text{m}$  diameter) to LAMP1 surfaces was calculated and co-localization was determined as distances <0.3  $\mu\text{m}$ .

For all other immunostaining, intestinal tissue was fixed in 10% neutral buffered formalin. Antigen retrieval was performed on 5  $\mu\text{m}$  tissue sections using Tris- or citric acid-based antigen unmasking solutions (Vector Laboratories, Burlington, Ontario). Sections were blocked in 10% normal goat serum and incubated with primary antibodies against CC3 (Cell Signaling, Beverly, MA), ZO-1 (Santa Cruz, Dallas, TX) and/or GFP (Abcam, Cambridge, MA). For immunofluorescent staining, samples were processed as described above. For immunohistochemical staining, sections were incubated with a horseradish peroxidase-conjugated anti-rabbit IgG secondary (Vector Laboratories), developed using a 3,3'-diaminobenzidine solution (Vector Laboratories), counterstained with hematoxylin, and mounted in Cytoseal XYL (Thermo Scientific, Waltham, MA). Late stage apoptotic cells were detected using the Click-iT Plus TUNEL assay (Invitrogen, Waltham, MA)

Fluorescent images were captured on an inverted DMI8 microscope (Leica, Buffalo Grove, IL) equipped with a CSU-W1 spinning disk, ZYLA SL150 sCMOS camera (Andor, South Windsor, CT),  $\times 20/0.40$  CORR, PL APO  $\times 40/0.85$  dry objectives, a  $\times 100/1.40-0.70$  oil objective, and iQ3 acquisition software (Andor). Brightfield microscopy was performed using a BZ-X710 with a  $\times 20/0.75$  PL APO dry objective, and BZ-X Viewer acquisition software (Keyence, Elmwood Park, NJ).

### Electron microscopy

Whole pieces of mouse jejunum were harvested and fixed overnight at 4°C in a solution of 2.5% glutaraldehyde, 2% paraformaldehyde, and 0.1M sodium cacodylate pH 7.4. Tissue was then post-fixed with 1% osmium tetroxide in 0.1 M sodium cacodylate buffer, stained en-bloc with 1% aqueous uranyl acetate, and dehydrated through a graded series of ethanol and propylene oxide. Next, tissues were incubated in a 1:1 mixture of EMBED 812 (Electron Microscopy Sciences 14120) and propylene oxide, then left in 100% EMBED 812 overnight before being embedded. Ultrathin sections (~70 nm) were cut, and grids were stained with uranyl acetate and lead citrate. Sections were imaged using a ThermoFisher Tecnai 12 transmission electron microscope and micrographs were recorded using a Gatan OneView 16-megapixel camera.

### IEL isolation and flow cytometry

Small intestinal IELs were isolated as previously described<sup>27</sup> and stained using fixable viability dye (eFluor 450 or 780, eBioscience), anti-CD3 (2C11, BioLegend), anti-TCR $\gamma\delta$  (GL3, BioLegend), and anti-TCR $\beta$  (H57-597, BioLegend). Flow cytometry was performed on an LSR II (BD Biosciences, Franklin Lakes, NJ) in the New Jersey Medical School Flow Cytometry and Immunology Core Laboratory and the data were analyzed by FlowJo (v. 10.4.2; Tree Star).

### Quantitative PCR

Intestinal epithelial cells were isolated by inverting a segment of mouse jejunum on a feeding needle and incubated in Cell Recovery Solution (Corning). Epithelial cells were pelleted and resuspended in Trizol (Life Technologies) and homogenized using a 23½ gauge needle. RNA was isolated with a RNeasy kit (Qiagen, Germantown, MD) and cDNA was generated using the iScript cDNA Synthesis Kit (Bio-Rad, Hercules, CA). qPCR was performed on the QuantStudio 6 Real-Time PCR System (Applied Biosystems, Beverly, MA) using PowerUp SYBR Green Master Mix (Applied Biosystems) and primers for *H60* (forward, 5'-GAGCCACCAGCAAGAGCAA-3'; reverse, 5'-CCAGTATGGTCCCCAGATAGCT-3'), *Rae1* (forward, 5'-ATCAACTTCCCCGCTTCCA-3'; reverse, 5'-AGATATGAAGATGAGTCCCACAGAGATA-3'), *Ulp1* (forward, 5'-TTCACATAGTGCAGGAGACTAACACA-3'; reverse, 5'-ACTGGCCACACACCTCAGC-3') (Li et al. 2012), or *Gapdh* (forward, 5'-AAGGTGGTGAAGCAGGCATCTGAG-3'; reverse, 5'-GGAAGAGTGGGAGTTGCTGTTGAAGTC3'). Fold changes were calculated using Ct values normalized to *Gapdh* expression.

**ELISA**

Whole pieces of mouse jejunum were homogenized with a bead beater in Bio-Plex Cell Lysis buffer (Bio-Rad). Protein concentrations were determined using the DC Protein Assay (Bio-Rad) and TNF levels were quantified using a mouse TNF ELISA kit (BioLegend) according to manufacturer instructions.

Sort-purified  $\gamma\delta$  or  $\alpha\beta$  IELs were seeded at approximately 400K cells per well in round-bottom 96-well plates coated with 2  $\mu\text{g/ml}$  anti-CD3 (145-2C11, BioLegend), 2  $\mu\text{g/ml}$  polyclonal Armenian hamster IgG (BioXCell, Lebanon, NH), and/or 2.5  $\mu\text{g/ml}$  E-cadherin-Fc (Sigma, St. Louis, MO). IELs were plated in RPMI-T medium containing 2  $\mu\text{g/ml}$  PerCP-e710 conjugated anti-CD107a (1D4B, Invitrogen) for 90 min. Granzyme A and B release were measured by ELISA (Abcam, Invitrogen). CD107a externalization was measured by flow cytometry as described above.

**scRNA sequencing data analysis**

Raw fastq files were downloaded from NCBI GEO (GSE157477), and subsequently aligned to the reference genome (GRCh38) via cellranger (v3.1.0). All subsequent processing was performing within the Seurat (v3.1.5) package. Low quality cells (percent mitochondrial reads/cell >15%, percent ribosomal reads/cell >45%, <500 feature counts or >3000 feature counts) were filtered from the dataset, and read counts were normalized using scTransform (citation: <https://genomebiology.biomedcentral.com/articles/10.1186/s13059-019-1874-1>). Samples were integrated to remove batch effects with the Seurat integrate function (citation: [https://www.cell.com/cell/fulltext/S0092-8674\(19\)30559-8](https://www.cell.com/cell/fulltext/S0092-8674(19)30559-8)), and clustered via UMAP according to nearest neighbors. A Wilcoxon rank sum test with FDR p-value adjustment was performed with  $P < 0.0001$ .

**Supplementary Figure Legends****Supplementary Figure 1. CD103 regulates  $\gamma\delta$  IEL migratory behavior to facilitate LPS-induced shedding of apoptotic enterocytes independent of the microbiome.**

(A) Quantification of CC3<sup>+</sup> shedding events in the duodenum and ileum of LPS-treated WT and CD103 KO mice. (B) Villus length in WT and CD103 KO mice. n=6 mice. (C) Frequency of CC3<sup>+</sup> and CC3<sup>-</sup> funnels in the jejunum of LPS-treated WT and CD103 KO mice. n=4-5 mice. (D) Quantification of PI<sup>+</sup> cells in LPS-treated WT and CD103 KO mice or FlaTox-treated WT mice. (E) Number of CC3<sup>+</sup> shedding events in the jejunum of cohoused WT and CD103 KO mice following LPS exposure. (F) Mean track speed of WT or CD103 KO  $\gamma\delta$  IELs that do or do not contact shedding cells (9-17 tracks). (G) Immunostaining for rat IgG (red), showing anti-CD103 on the surface of  $\gamma\delta$  IELs (green). White: F-actin. Scale bar = 25  $\mu$ m. n = 3-6 mice. (H) Ratio of TCR $\beta$ <sup>+</sup> to TCR $\delta$ <sup>+</sup> IELs in whole small intestine as determined by flow cytometry. Gated on live CD3<sup>+</sup> cells. n = 7-8 mice. \**P* < .05, \*\**P* < .01, \*\*\**P* < .001.

**Supplementary Figure 2. Diphtheria toxin effectively depletes  $\gamma\delta$  IELs in TcrdGDL mice**

WT or TcrdGDL mice were treated with diphtheria toxin (DT) or vehicle control prior to PBS or LPS treatment. (A) Representative flow cytometry plots showing the (B) percent of TCR $\gamma\delta$ <sup>+</sup> IELs in the small intestine, gated on live CD3<sup>+</sup> cells. (C) Quantification of CC3<sup>+</sup> shedding events in jejunal tissue. n = 2-5 mice.

**Supplementary Figure 3. Signaling through TCR $\gamma\delta$  or NKG2D is not required for LPS-induced cell shedding.**

(A) Quantification of CC3 staining in mice treated with anti-TCR $\gamma\delta$  or IgG control prior to LPS administration. (B-D) RNA expression of NKG2D ligands (MULT1, RAE1, and H60) in jejunal epithelium isolated from PBS- or LPS-treated WT mice. Data are shown as the fold change in expression relative to control mice. (E) Quantification of CC3 staining of jejunum from mice administered NKG2D blocking antibody or IgG control prior to LPS exposure. n = 3-6 mice; n.s., not significant.

**Supplementary Figure 4. Granzyme-deficient bone marrow chimeras exhibit reduced shedding of apoptotic enterocytes following LPS treatment.**

(A) Ratio of TCR $\beta$ <sup>+</sup> to TCR $\delta$ <sup>+</sup> IELs in whole small intestine as determined by flow cytometry in Gzm KO chimeras or (B) mixed bone marrow chimeras. Gated on live CD3<sup>+</sup> cells. n = 3-15 mice. (C) Number of TUNEL<sup>+</sup> cells in the jejunum

of LPS-treated WT and GzmA/B KO mixed bone marrow chimeras. (D) Quantification of CC3<sup>+</sup> shedding events in the ileal sections from LPS-treated WT and GzmA/B KO mice. (E) Quantification of PI<sup>+</sup> cells in the jejunum of LPS-treated GzmA/B KO mice. Dashed line represents the average number of positive cells in WT mice. n=3 mice.

**Supplementary Figure 5. The number of cleaved caspase-3 apoptotic enterocytes are increased in CD biopsies.**

Quantification of (A) average CC3 staining within 5 villi or (B) total CC3 staining in enterocytes surrounding all IELs from duodenal and ileal biopsies with normal histology, quiescent or active CD. n=4-9 patients. \**P* < .05, \*\**P* < .01, \*\*\**P* < .01

**Supplementary Table 1. Cohort characteristics for duodenal biopsies**

**Supplementary Table 2. Cohort characteristics for ileal biopsies**

**Video Legends**

**Supplementary Video 1.** Intravital imaging of  $\gamma\delta$  T cells (green), luminal Alexa Fluor 633 (red) and nuclei (white) in jejunum of a TcrdEGFP mouse treated with 10mg/kg LPS for 90 min. Frames were collected every 30 s.

**Supplementary Video 2.** Intravital imaging of  $\gamma\delta$  T cells (green), APC-conjugated anti-CD8 $\alpha$  (white) and nuclei (magenta) in jejunum of a TcrdEGFP mouse treated with 10mg/kg LPS for 90 min. Frames were collected every 24 s.

**Supplementary Video 3.** Intravital imaging and 3D reconstruction of a  $\gamma\delta$  T cell (green) directly interacting with a ZO-1 funnel (white) in the jejunum of an LPS-treated TcrdGDL; mRFP-ZO-1 Tg mouse. Frames were collected every 17 s.

## **Supplementary Methods**

### **Immunofluorescent and immunohistochemical staining**

Frozen sections, 5  $\mu\text{m}$  thick, of fixed mouse intestine were obtained as previously described<sup>17</sup> and immunostained with Alexa Fluor 594-conjugated anti-Rat IgG, Alexa Fluor 647-conjugated phalloidin and Hoechst 33342 (Life Technologies, Waltham, MA). Slides were mounted with Prolong Glass (Life Technologies).

To visualize granzymes and vesicles within IELs, small intestinal IELs were isolated, sort-purified, fixed and permeabilized with Cytotfix/Cytoperm (BD Biosciences, Franklin Lakes, NJ) and stained with antibodies against Granzyme A, Granzyme B, LAMP1 (BioLegend, San Diego, CA). The appropriate secondary antibodies and Hoechst 33342 (Life Technologies) were applied, and the cells were affixed to glass slides by cytocentrifugation and mounted in Prolong Glass (Life Technologies). Co-localization was determined by generating surfaces for LAMP1 and spots for Gzm<sup>+</sup> vesicles using Imaris (v. 9.7.1; Bitplane, South Windsor, CT). Surfaces were generated to demarcate individual cells for vesicle classification. The distance between Gzm spots (0.35 $\mu\text{m}$  diameter) to LAMP1 surfaces was calculated and co-localization was determined as distances <0.3  $\mu\text{m}$ .

For all other immunostaining, intestinal tissue was fixed in 10% neutral buffered formalin. Antigen retrieval was performed on 5  $\mu\text{m}$  tissue sections using Tris- or citric acid-based antigen unmasking solutions (Vector Laboratories, Burlington, Ontario). Sections were blocked in 10% normal goat serum and incubated with primary antibodies against CC3 (Cell Signaling, Beverly, MA), ZO-1 (Santa Cruz, Dallas, TX) and/or GFP (Abcam, Cambridge, MA). For immunofluorescent staining, samples were processed as described above. For immunohistochemical staining, sections were incubated with a horseradish peroxidase-conjugated anti-rabbit IgG secondary (Vector Laboratories), developed using a 3,3'-diaminobenzidine solution (Vector Laboratories), counterstained with hematoxylin, and mounted in Cytoseal XYL (Thermo Scientific, Waltham, MA). Late stage apoptotic cells were detected using the Click-iT Plus TUNEL assay (Invitrogen, Waltham, MA)

Fluorescent images were captured on an inverted DMI8 microscope (Leica, Buffalo Grove, IL) equipped with a CSU-W1 spinning disk, ZYLA SL150 sCMOS camera (Andor, South Windsor, CT),  $\times 20/0.40$  CORR, PL APO  $\times 40/0.85$  dry objectives, a  $\times 100/1.40-0.70$  oil objective, and iQ3 acquisition software (Andor). Brightfield microscopy was performed using a BZ-X710 with a  $\times 20/0.75$  PL APO dry objective, and BZ-X Viewer acquisition software (Keyence, Elmwood Park, NJ).

### Electron microscopy

Whole pieces of mouse jejunum were harvested and fixed overnight at 4°C in a solution of 2.5% glutaraldehyde, 2% paraformaldehyde, and 0.1M sodium cacodylate pH 7.4. Tissue was then post-fixed with 1% osmium tetroxide in 0.1 M sodium cacodylate buffer, stained en-bloc with 1% aqueous uranyl acetate, and dehydrated through a graded series of ethanol and propylene oxide. Next, tissues were incubated in a 1:1 mixture of EMBED 812 (Electron Microscopy Sciences 14120) and propylene oxide, then left in 100% EMBED 812 overnight before being embedded. Ultrathin sections (~70 nm) were cut, and grids were stained with uranyl acetate and lead citrate. Sections were imaged using a ThermoFisher Tecnai 12 transmission electron microscope and micrographs were recorded using a Gatan OneView 16-megapixel camera.

### IEL isolation and flow cytometry

Small intestinal IELs were isolated as previously described<sup>27</sup> and stained using fixable viability dye (eFluor 450 or 780, eBioscience), anti-CD3 (2C11, BioLegend), anti-TCR $\gamma\delta$  (GL3, BioLegend), and anti-TCR $\beta$  (H57-597, BioLegend). Flow cytometry was performed on an LSR II (BD Biosciences, Franklin Lakes, NJ) in the New Jersey Medical School Flow Cytometry and Immunology Core Laboratory and the data were analyzed by FlowJo (v. 10.4.2; Tree Star).

### Quantitative PCR

Intestinal epithelial cells were isolated by inverting a segment of mouse jejunum on a feeding needle and incubated in Cell Recovery Solution (Corning). Epithelial cells were pelleted and resuspended in Trizol (Life Technologies) and homogenized using a 23½ gauge needle. RNA was isolated with a RNeasy kit (Qiagen, Germantown, MD) and cDNA was generated using the iScript cDNA Synthesis Kit (Bio-Rad, Hercules, CA). qPCR was performed on the QuantStudio 6 Real-Time PCR System (Applied Biosystems, Beverly, MA) using PowerUp SYBR Green Master Mix (Applied Biosystems) and primers for *H60* (forward, 5'-GAGCCACCAGCAAGAGCAA-3'; reverse, 5'-CCAGTATGGTCCCCAGATAGCT-3'), *Rae1* (forward, 5'-ATCAACTTCCCCGCTTCCA-3'; reverse, 5'-AGATATGAAGATGAGTCCCACAGAGATA-3'), *Ubp1* (forward, 5'-TTCACATAGTGCAGGAGACTAACACA-3'; reverse, 5'-ACTGGCCACACACCTCAGC-3') (Li et al. 2012), or *Gapdh* (forward, 5'-AAGGTGGTGAAGCAGGCATCTGAG-3'; reverse, 5'-GGAAGAGTGGGAGTTGCTGTTGAAGTC3'). Fold changes were calculated using Ct values normalized to *Gapdh* expression.

**ELISA**

Whole pieces of mouse jejunum were homogenized with a bead beater in Bio-Plex Cell Lysis buffer (Bio-Rad). Protein concentrations were determined using the DC Protein Assay (Bio-Rad) and TNF levels were quantified using a mouse TNF ELISA kit (BioLegend) according to manufacturer instructions.

Sort-purified  $\gamma\delta$  or  $\alpha\beta$  IELs were seeded at approximately 400K cells per well in round-bottom 96-well plates coated with 2  $\mu\text{g/ml}$  anti-CD3 (145-2C11, BioLegend), 2  $\mu\text{g/ml}$  polyclonal Armenian hamster IgG (BioXCell, Lebanon, NH), and/or 2.5  $\mu\text{g/ml}$  E-cadherin-Fc (Sigma, St. Louis, MO). IELs were plated in RPMI-T medium containing 2  $\mu\text{g/ml}$  PerCP-e710 conjugated anti-CD107a (1D4B, Invitrogen) for 90 min. Granzyme A and B release were measured by ELISA (Abcam, Invitrogen). CD107a externalization was measured by flow cytometry as described above.

**scRNA sequencing data analysis**

Raw fastq files were downloaded from NCBI GEO (GSE157477), and subsequently aligned to the reference genome (GRCh38) via cellranger (v3.1.0). All subsequent processing was performing within the Seurat (v3.1.5) package. Low quality cells (percent mitochondrial reads/cell >15%, percent ribosomal reads/cell >45%, <500 feature counts or >3000 feature counts) were filtered from the dataset, and read counts were normalized using scTransform (citation: <https://genomebiology.biomedcentral.com/articles/10.1186/s13059-019-1874-1>). Samples were integrated to remove batch effects with the Seurat integrate function (citation: [https://www.cell.com/cell/fulltext/S0092-8674\(19\)30559-8](https://www.cell.com/cell/fulltext/S0092-8674(19)30559-8)), and clustered via UMAP according to nearest neighbors. A Wilcoxon rank sum test with FDR p-value adjustment was performed with  $P < 0.0001$ .

**Supplementary Figure Legends****Supplementary Figure 1. CD103 regulates  $\gamma\delta$  IEL migratory behavior to facilitate LPS-induced shedding of apoptotic enterocytes independent of the microbiome.**

(A) Quantification of CC3<sup>+</sup> shedding events in the duodenum and ileum of LPS-treated WT and CD103 KO mice. (B) Villus length in WT and CD103 KO mice. n=6 mice. (C) Frequency of CC3<sup>+</sup> and CC3<sup>-</sup> funnels in the jejunum of LPS-treated WT and CD103 KO mice. n=4-5 mice. (D) Quantification of PI<sup>+</sup> cells in LPS-treated WT and CD103 KO mice or FlaTox-treated WT mice. (E) Number of CC3<sup>+</sup> shedding events in the jejunum of cohoused WT and CD103 KO mice following LPS exposure. (F) Mean track speed of WT or CD103 KO  $\gamma\delta$  IELs that do or do not contact shedding cells (9-17 tracks). (G) Immunostaining for rat IgG (red), showing anti-CD103 on the surface of  $\gamma\delta$  IELs (green). White: F-actin. Scale bar = 25  $\mu$ m. n = 3-6 mice. (H) Ratio of TCR $\beta$ <sup>+</sup> to TCR $\delta$ <sup>+</sup> IELs in whole small intestine as determined by flow cytometry. Gated on live CD3<sup>+</sup> cells. n = 7-8 mice. \**P* < .05, \*\**P* < .01, \*\*\**P* < .001.

**Supplementary Figure 2. Diphtheria toxin effectively depletes  $\gamma\delta$  IELs in TcrdGDL mice**

WT or TcrdGDL mice were treated with diphtheria toxin (DT) or vehicle control prior to PBS or LPS treatment. (A) Representative flow cytometry plots showing the (B) percent of TCR $\gamma\delta$ <sup>+</sup> IELs in the small intestine, gated on live CD3<sup>+</sup> cells. (C) Quantification of CC3<sup>+</sup> shedding events in jejunal tissue. n = 2-5 mice.

**Supplementary Figure 3. Signaling through TCR $\gamma\delta$  or NKG2D is not required for LPS-induced cell shedding.**

(A) Quantification of CC3 staining in mice treated with anti-TCR $\gamma\delta$  or IgG control prior to LPS administration. (B-D) RNA expression of NKG2D ligands (MULT1, RAE1, and H60) in jejunal epithelium isolated from PBS- or LPS-treated WT mice. Data are shown as the fold change in expression relative to control mice. (E) Quantification of CC3 staining of jejunum from mice administered NKG2D blocking antibody or IgG control prior to LPS exposure. n = 3-6 mice; n.s., not significant.

**Supplementary Figure 4. Granzyme-deficient bone marrow chimeras exhibit reduced shedding of apoptotic enterocytes following LPS treatment.**

(A) Ratio of TCR $\beta$ <sup>+</sup> to TCR $\delta$ <sup>+</sup> IELs in whole small intestine as determined by flow cytometry in Gzm KO chimeras or (B) mixed bone marrow chimeras. Gated on live CD3<sup>+</sup> cells. n = 3-15 mice. (C) Number of TUNEL<sup>+</sup> cells in the jejunum

of LPS-treated WT and GzmA/B KO mixed bone marrow chimeras. (D) Quantification of CC3<sup>+</sup> shedding events in the ileal sections from LPS-treated WT and GzmA/B KO mice. (E) Quantification of PI<sup>+</sup> cells in the jejunum of LPS-treated GzmA/B KO mice. Dashed line represents the average number of positive cells in WT mice. n=3 mice.

**Supplementary Figure 5. The number of cleaved caspase-3 apoptotic enterocytes are increased in CD biopsies.**

Quantification of (A) average CC3 staining within 5 villi or (B) total CC3 staining in enterocytes surrounding all IELs from duodenal and ileal biopsies with normal histology, quiescent or active CD. n=4-9 patients. \**P* < .05, \*\**P* < .01, \*\*\**P* < .01

**Supplementary Table 1. Cohort characteristics for duodenal biopsies**

**Supplementary Table 2. Cohort characteristics for ileal biopsies**

**Video Legends**

**Supplementary Video 1.** Intravital imaging of  $\gamma\delta$  T cells (green), luminal Alexa Fluor 633 (red) and nuclei (white) in jejunum of a TcrdEGFP mouse treated with 10mg/kg LPS for 90 min. Frames were collected every 30 s.

**Supplementary Video 2.** Intravital imaging of  $\gamma\delta$  T cells (green), APC-conjugated anti-CD8 $\alpha$  (white) and nuclei (magenta) in jejunum of a TcrdEGFP mouse treated with 10mg/kg LPS for 90 min. Frames were collected every 24 s.

**Supplementary Video 3.** Intravital imaging and 3D reconstruction of a  $\gamma\delta$  T cell (green) directly interacting with a ZO-1 funnel (white) in the jejunum of an LPS-treated TcrdGDL; mRFP-ZO-1 Tg mouse. Frames were collected every 17 s.